applied sciences

MDPI

Article

Mechanical Response Analysis of a Tunnel-First Subway Station Constructed with Circumferential Pipe Curtain Pre-Support

Xiaojing Sun [1,2], Meiwei Zheng [1,2,*], Hanfan Liu [1,2], Zhengquan Ding [2] and Huawei Guo [3]

[1] Key Laboratory of Urban Underground Engineering of Ministry of Education, Beijing Jiaotong University, Beijing 100044, China; xjsun1@bjtu.edu.cn (X.S.); 23121503@bjtu.edu.cn (H.L.)
[2] School of Civil Engineering, Beijing Jiaotong University, Beijing 100044, China; 23115145@bjtu.edu.cn
[3] China Railway Siyuan Survey and Design Group Co., Ltd., Wuhan 430063, China; 006893@crfsdi.com
* Correspondence: 24125992@bjtu.edu.cn

Abstract

A circumferential pipe curtain (CPC) pre-support method is examined for tunnel-first station construction using Baidang South Station as the engineering background. A three-dimensional FLAC3D model represents a three-stage, eight-step construction sequence, including excavation, segment removal, structural installation, and temporary-support removal. The analysis follows ground deformation and the responses of the pipe curtains, tunnel segments, and beam-column system. For the modeled condition, the reported final maximum surface settlement is 6.18 mm. Elevated tensile demand occurs near the segment–lower pipe-curtain connections and the upper longitudinal-beam corbels during different construction steps. Later reductions in some response quantities reflect redistribution within the simulated sequence. The results identify locations and operations for detailed connection assessment, construction-stage monitoring, and targeted design considerations.

Keywords: circumferential pipe curtain pre-support; tunnel-first method; numerical simulation; mechanical response; subway station

1. Introduction

In the construction of urban subways in China, the preferred method for building tunnels is shield tunneling. This method offers high safety and efficiency, minimal environmental impact and low overall costs [1–3]. However, station construction still relies on conventional cut-and-cover methods, mined methods, or a combination of both.

Currently, when the construction of shield-driven running tunnels and cut-and-cover or mined stations proceeds concurrently, two methods are commonly adopted. One of them is the station-first method, which can be further divided into two types based on the support modes: shield traversing through the primary support and shield traversing through the secondary lining. The second is the tunnel-first method. In this approach, the shield machine excavates directly through the station area and the segmental lining is dismantled later to construct the station.

As China's urban rail transit network continues to expand, the tunnel-first method is becoming increasingly important for development in complex urban environments. This method avoids the need for surface demolition, reduces traffic disruption and minimizes the impact on sensitive adjacent structures. It also prevents resource waste and efficiency losses caused by mismatched construction schedules between stations and running tunnels [4,5].

In the early development of the tunnel-first method, construction typically combined shield tunneling with either the cross-passage method [6] or the underpinning beam

Check for updates

Received: 16 October 2026
Revised: 26 November 2026
Accepted: 27 November 2026
Published: 29 November 2026

Copyright: © 2026 by the authors. Licensee MDPI, Basel, Switzerland. This article is an open access article distributed under the terms and conditions of the Creative Commons Attribution (CC BY) license.

method [7,8]. This approach involved installing temporary support within the existing tunnel, followed by localized expansion excavation.

With the development of urban underground space, combining shield tunneling with the mined method [9] has gradually become mainstream. Zhou et al. [10] investigated the in situ expansion of a subway tunnel into a station using blasting techniques. Based on a real engineering project, they conducted numerical simulations to analyze the drilling and blasting process. Their study evaluated several key aspects, including the over-excavation and under-excavation profiles, the blasting response during tunnel expansion, the rock stress evolution induced by shock waves, and the vibration velocity of the surrounding rock. The proposed blasting parameters successfully maintained a smooth tunnel cross-section and ensured controllable over-and under-excavation quality.

Furthermore, Liu et al. [11] proposed a column-type underground station construction method that integrates shield tunneling with shallow tunneling method. Their model tests successfully verified the structural safety and stability of this method during construction.

In recent years, the combination of shield tunneling and the Pile-Beam-Arch (PBA) method [12,13] has emerged as a significant technological innovation. This approach provides better control over structural deformation in complex urban environments. In this field, Sedghi and Golshani [14] conducted 3D numerical analyses using FLAC3D. They quantitatively evaluated the surface settlement induced by PBA construction and the mitigation of secondary damage to adjacent existing buildings.

During large-section mined excavation using the tunnel-first method, advance support systems are essential for controlling ground settlement and preventing instability. These technical methods continually evolve to meet engineering demands. Zhang [15] clarified the core mechanical mechanism of traditional advance rock bolts, which act as active supports. He demonstrated how they effectively mobilize and augment the load-bearing capacity of the surrounding rock.

Chen et al. [16] investigated various anchoring systems in layered rock masses via laboratory tests. They found that rock bolts function through two combined mechanisms. First, the anchoring agent restores cohesion in the rock mass surrounding the borehole. Second, the bolt body provides support resistance. Notably, fully grouted bolts significantly enhance the load-bearing capacity of the rock mass.

Furthermore, Wu et al. [17] combined numerical simulations with field verifications to study high-prestress rock bolts. They evaluated the mechanical behavior and stability control of the surrounding rock in deep roadways. Their research analyzed the energy balance criteria, fracture evolution and energy dissipation of anchored rock masses under uniaxial compression at various levels of prestress. Advance small pipe grouting and pipe roof technologies [18] are widely used in weaker strata. These technologies consolidate loose rock masses into an integral, load-bearing structure. Furthermore, Zhang et al. [19] revealed how the spacing and layout of these pipes affects support efficacy.

To address special geological and environmental constraints, innovative techniques combining parallel pipe curtains [20] or freeze-sealing pipe roof method have emerged. Guan et al. [21] used a combination of numerical simulations and field measurements to evaluate shield tunnel excavation. They found that deformation of the segments in the unfrozen layers was three times greater than in the frozen layers. Additionally, surface settlement above the frozen layer was under 2 mm. Notably, buildings farther from the frozen zone experienced greater vertical settlement than those closer to it. Hong et al. [22] developed a 3D thermo-mechanical coupled numerical model to analyze temperature distribution during different freezing stages. This model effectively evaluated the mechanical impact of frost heave on existing structures. Taking the Taiyuan Railway Station underpass tunnel as a case study, Yang et al. [23] combined numerical simulations and model tests.

They investigated the surface settlement characteristics of a pre-constructed closed pipe curtain tunnel during the pipe jacking phase.

Advance pipe roofs are the preferred choice for projects involving larger spans and stricter settlement control requirements. This is due to their greater stiffness and ability to support longer distances [24,25]. Fu et al. [26] demonstrated that ultra-long pipe roofs can significantly reduce the disturbance caused by excavation to adjacent subgrades and pile foundations. This mitigation is achieved through distinct arching and interlocking effects. To comprehensively isolate large-span excavations, pipe curtain pre-support technology uses interlocking large-diameter steel pipes to form a continuous load-bearing shell. Zhang et al. [27] used stress-deflection theory to comprehensively analyze the deformation mechanism of transverse pipe curtains and their control over strata relaxation. Meanwhile, the mechanical pre-cutting method [28] forms a rigid arch shell prior to excavation.

Based on the Siqiao Station project of Hangzhou Metro Line 9 in China, Li et al. [29] proposed and validated a "0-θ tunneling method" integrating quasi-rectangular shield tunneling and pipe jacking. Bai et al. [30] developed a deformation prediction model for pipe curtains, compared it with field monitoring data, and examined the effects of arrangement parameters.

Based on the preceding analysis, traditional advance support methods, such as pipe roofs and advance small pipes, are predominantly used when expanding the main station structure in tunnel-first projects. These support components are typically linear and installed longitudinally. During construction, the spatial cavity formed by the completed shield tunnel is not fully utilized. Instead, newly exposed excavation faces are repeatedly created, increasing the number of construction steps and prolonging the overall schedule. Furthermore, multiple partial excavations can easily exacerbate disturbances to weak strata, thereby triggering surface settlement.

Drawing on the engineering background of Baidang South Station on Suzhou Rail Transit Line 7, this paper presents a novel technique: the circumferential pipe curtain pre-support (CPC) method. It also examines surface settlement characteristics during construction using the new tunnel-first subway station construction method using circumferential pipe curtain pre-support. The study also analyses the mechanical response characteristics of the circumferential pipe curtains, shield segments and station beam-column structures. By identifying the structural weak points of the station and running tunnel, this research provides a crucial basis for successfully implementing the CPC method.

2. A Novel Tunnel-First Subway Station Construction Method Using Circumferential Pipe Curtain Pre-Support

2.1. Structural Configuration of the Station

Baidang South Station on Suzhou Rail Transit Line 7 provides the engineering background for this numerical investigation. As shown in Figure 1, the standard structural cross-section consists of the permanent shield tunnel segments, upper and lower circumferential pipe curtains, a beam-column system, and the secondary linings within both the station and the tunnel.

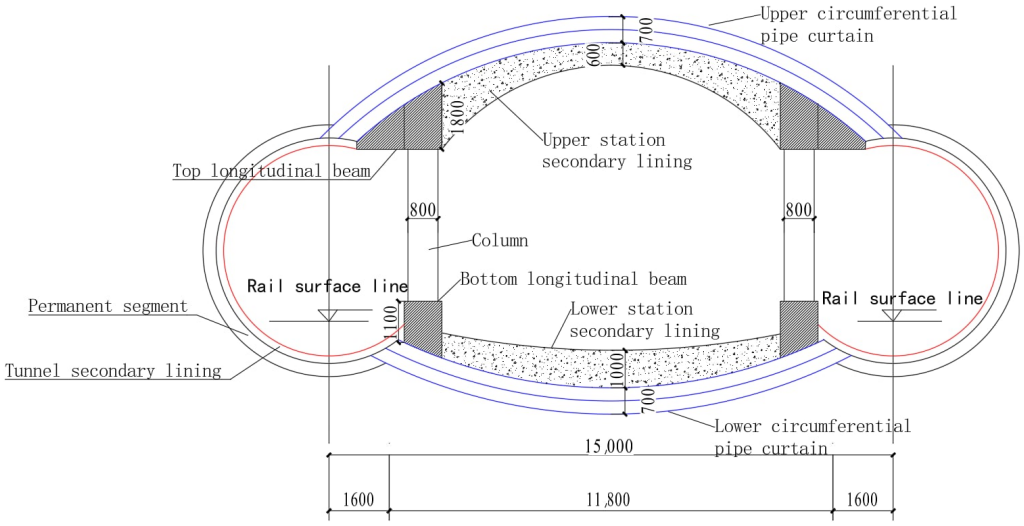


Figure 1. Station structural design.

For the running tunnel, the segments have an outer diameter of 6700 mm and a thickness of 350 mm. The internal secondary lining is 200 mm thick. The upper and lower circumferential pipe curtains have a diameter of 700 mm, with the crown of the upper curtain buried at a depth of 15 m.

The secondary lining of the main station structure has a variable thickness. The upper secondary lining is 600 mm thick at its center, while its ends match the 1800 mm height of the top longitudinal beams. Furthermore, the lower secondary lining is 1000 mm thick at the center and 650 mm thick at both ends.

Regarding materials, the circumferential pipe curtains use Q355B steel filled with C50 concrete. The secondary linings, the trapezoidal top and bottom longitudinal beams are made of C40 concrete, whereas the permanent columns utilize C50 concrete. These permanent columns have an 800 mm × 1200 mm cross-section, with longitudinal and transverse spacings of 9 m and 10 m, respectively.

2.2. Component Design

2.2.1. Circumferential Pipe Curtain Design

In the circumferential pipe curtain method, the completed shield tunnel is used as a launch space. Steel pipes are jacked into the soil along a predetermined curved path and then docked precisely within the adjacent, parallel tunnel. This forms a closed, arched circumferential pipe curtain pre-support in the unexcavated area between the tunnels.

The proposed arrangement forms a continuous pre-support system before mined excavation and is intended to restrain ground deformation. Its configuration is illustrated in Figure 2.

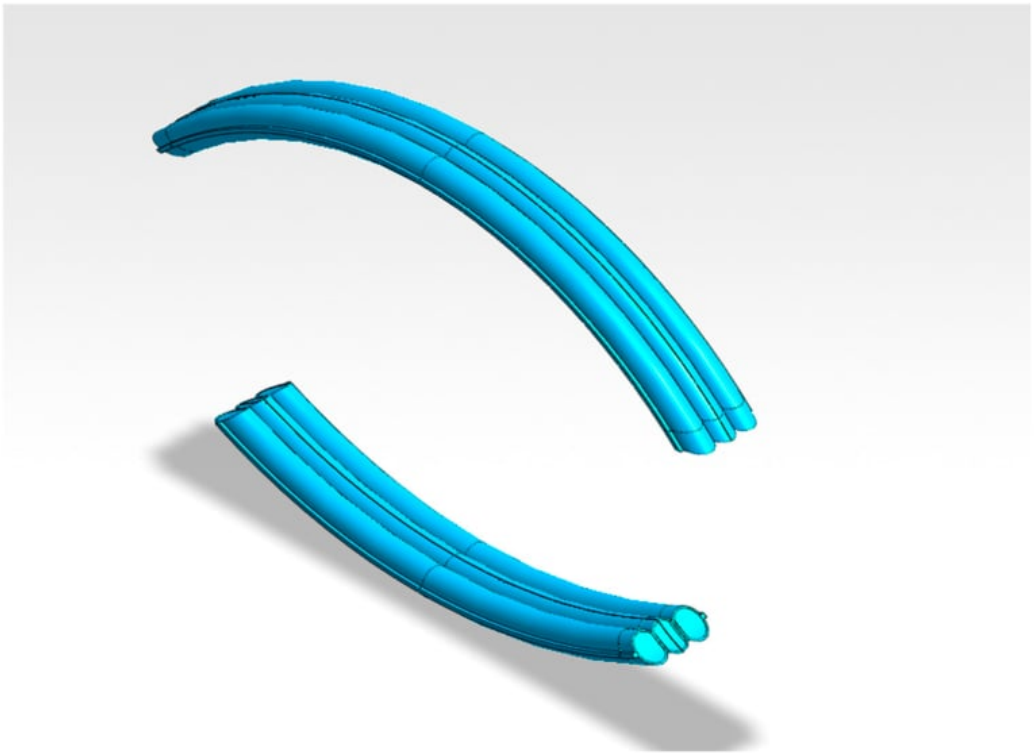


Figure 2. Structure of the circumferential pipe curtain.

The circumferential pipe curtain uses a triple-circular-pipe composite structure. The steel pipes have an outer diameter of 700 mm, a center-to-center spacing of 570 mm, and a wall thickness of 20 mm.The cross-section of the pipe curtain and the arrangement of the triple-pipe units are shown in Figure 3.

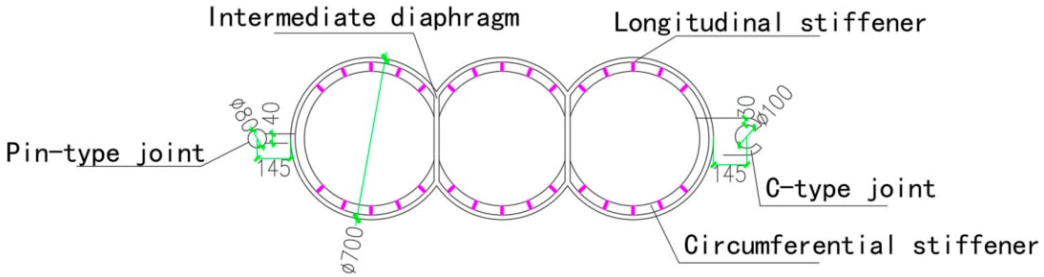


Figure 3. Cross-section of the circumferential pipe curtain (mm).

To enhance structural stiffness, transverse and longitudinal stiffening ribs are installed inside the pipes. Each triple-pipe unit is fabricated by integrally welding three individual steel pipes together.

Additionally, circumferential ribs with a height of 40 mm are installed at regular intervals along the pipes. These circumferential ribs are connected by longitudinal ribs, significantly improving the overall stiffness of the pipe curtain.

The upper circumferential pipe curtain has a curvature radius of 10.5 m and a jacking length of 15.983 m. Similarly, the lower circumferential pipe curtain features a curvature radius of 13.5 m and a jacking length of 12.424 m.

Several factors influence the pipe segmentation, including in-tunnel launching operations, construction welding, and guide rail installation. Consequently, the upper circumferential pipe curtain consists of standard segments (2.45 m) and short segments (1.283 m), as shown in Figure 4.

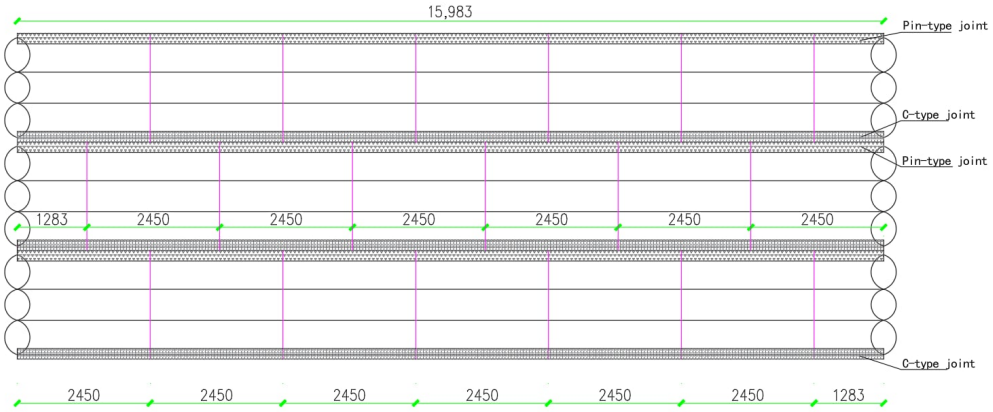


Figure 4. Unfolded view of the circumferential pipe curtain segments (mm).

These short segments are installed exclusively at the beginning or end of a sequence. Furthermore, each assembled pipe string contains only one short segment. This arrangement effectively staggers the structural joints.

The lower circumferential pipe curtain comprises standard segments (2.25 m) and short segments (1.174 m). Their overall layout and joint-staggering arrangement are identical to those of the upper curtain.

2.2.2. Shield Segment Design

The running tunnel segments within the cross-section are classified as either permanent or removable, as shown in Figure 5. The segments labelled A1–A3 and B1 are permanent, meaning they form part of the permanent load-bearing structure. In contrast, segments A4, B2 and the key segment (K block) are removable and are located within specific angular regions of the cross-section.

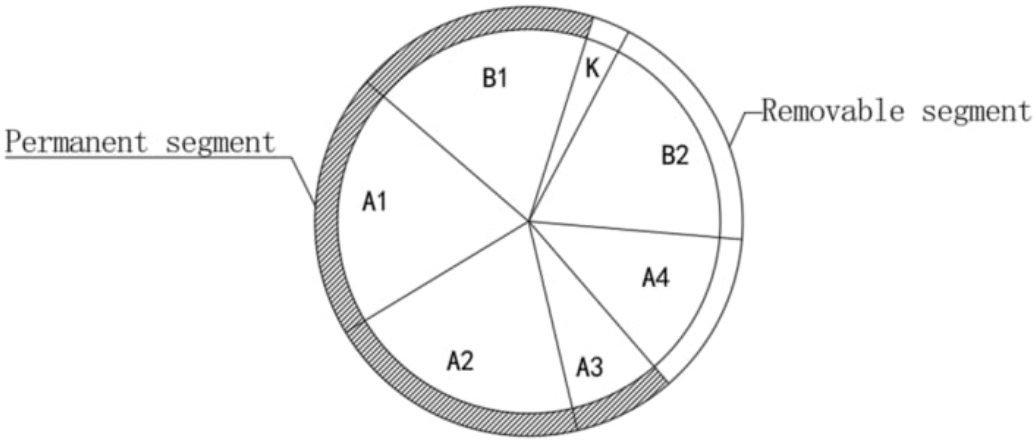


Figure 5. Segments of the running tunnel.

2.3. The "Three-Stage, Eight-Step" Construction Method

During the construction using the CPC method, the structural force system transition involves three key stages and eight steps:

(1) Stage 1: Initial shield tunneling and circumferential pipe curtain jacking (illustrated by S1–S3 in Figure 6)

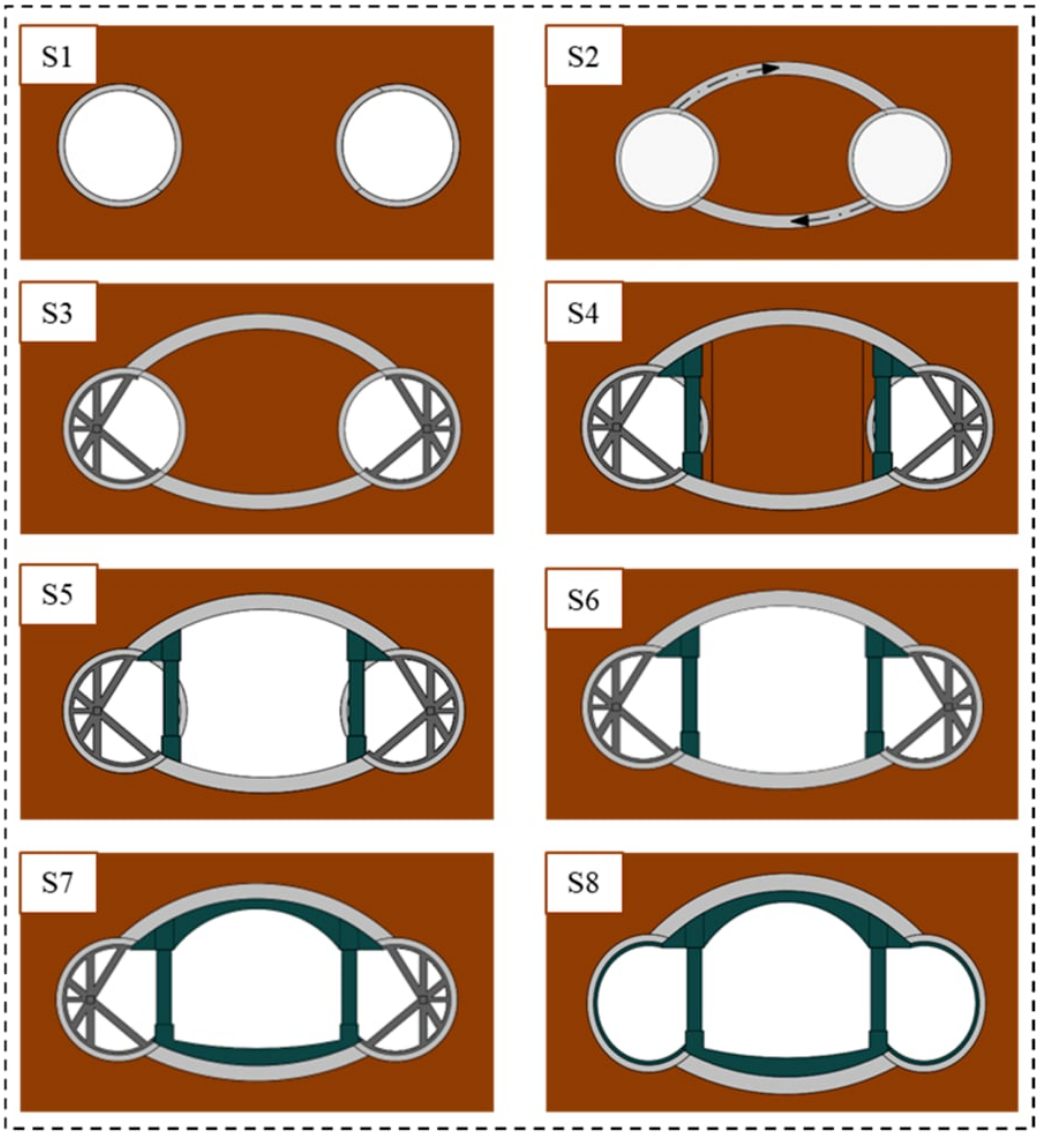


Figure 6. Construction flowchart of the CPC method.

Step S1: Complete shield excavation and breakthrough through the station area.

Step S2: Install the circumferential pipe curtains from the completed tunnel to establish pre-support before station excavation.

Step S3: Install the temporary supports inside the shield tunnels to restrain segment deformation during subsequent segment removal and station excavation.

(2) Stage 2: Main station structure formation and spatial connection (illustrated by S4–S6 in Figure 6)

Step S4: Remove the designated segments at column locations and install the corresponding local beam and column portions.

Step S5: Excavate the main station space in stages under the pipe-curtain support. The analyzed sequence uses the double-side drift scheme. Other excavation schemes are outside the present response analysis.

Step S6: Dismantle the remaining removable segments in sections. This establishes a complete spatial connection between the station space and the running tunnel space.

(3) Stage 3: Construction of secondary linings in the station and tunnel (illustrated by steps S7–S8 in Figure 6).

Step S7: Install the remaining longitudinal-beam portions and the station secondary lining to form the closed station structure.

Step S8: Remove the temporary tunnel supports in the adopted sequence after completion of the station lining and satisfaction of the applicable strength-acceptance condition, then install the tunnel secondary lining. The numerical activation sequence represents the change in structural configuration; concrete curing is not represented by an age-dependent material law.

3. Numerical Model

A three-dimensional finite-difference continuum model was constructed in FLAC3D using a mesh prepared in Midas GTS NX. The soil was represented as an isotropic, continuous, elastic–perfectly plastic material with the Mohr–Coulomb criterion. Structural continuum regions were assigned linear elastic behavior. The Mohr–Coulomb model was adopted as an engineering simplification for analysing the staged construction response. The model does not reproduce stress-dependent stiffness, small-strain nonlinearity, or post-yield hardening and softening; these limitations and their possible effects are discussed in Section 5.4.

The calculation represents a post-dewatering condition, with groundwater assumed to be at least 0.5 m below the structural base. Groundwater flow, pore-pressure coupling, and additional surface-building loads were not included. The initial stress state was generated from self-weight.

Excavation and structural removal were implemented by assigning the null constitutive model to predefined zone groups. Structural installation was represented by activating the corresponding regions with the elastic model and assigning bulk modulus, shear modulus, and density. Longitudinal ranges were used to advance the operations, with 2 m increments in pipe-curtain activation and predominantly 4 m increments in the station-excavation sequence, including staggered operations and shorter end sections.

The computational domain measures 180 m × 30 m × 50 m, with 15 m of cover above the upper pipe curtain, as shown in Figure 7. A hybrid mesh was used. The mesh size is set to 0.2 m for the circumferential pipe curtains and tunnel segments, and 0.3 m for the beam-column system and station secondary lining. For the soil mass, the mesh size is 0.5 m both inside the station and within a range of two times the tunnel diameter outside the excavation zone. At the far ends of the model, the mesh size transitions to 4 m. Local refinement represents the structural and connection geometry, with coarser zones in the far-field ground.

Regarding boundary conditions, the bottom surface of the model is fixed in all directions. Displacements in the X-direction are constrained at the left and right boundaries, while displacements in the Y-direction are constrained at the front and back boundaries.

The soil strata are simulated using the Mohr-Coulomb constitutive model, whereas the running tunnel and station structure materials are represented using a linear elastic model. The physical and mechanical parameters adopted in this model are listed in Tables 1 and 2. The soil parameters in Table 1 were selected primarily with reference to the detailed geotechnical investigation of the project site. The strata within the excavation influence zone were generalized into three representative engineering layers, layer1 to layer3, for the numerical analysis. As specified in Section 2.1, the longitudinal beams, including their corbels, are C40 concrete.

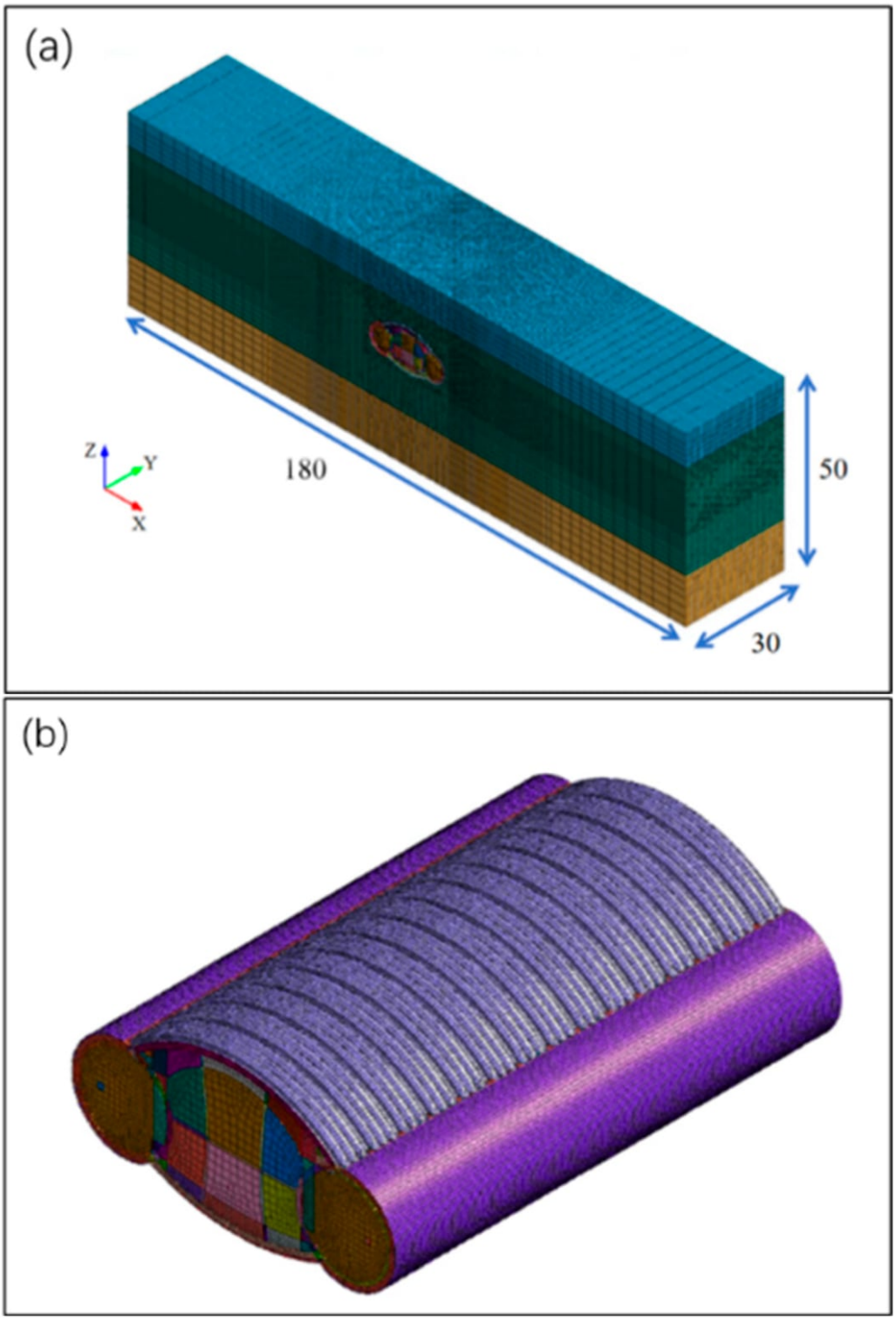


Figure 7. *Cont.*

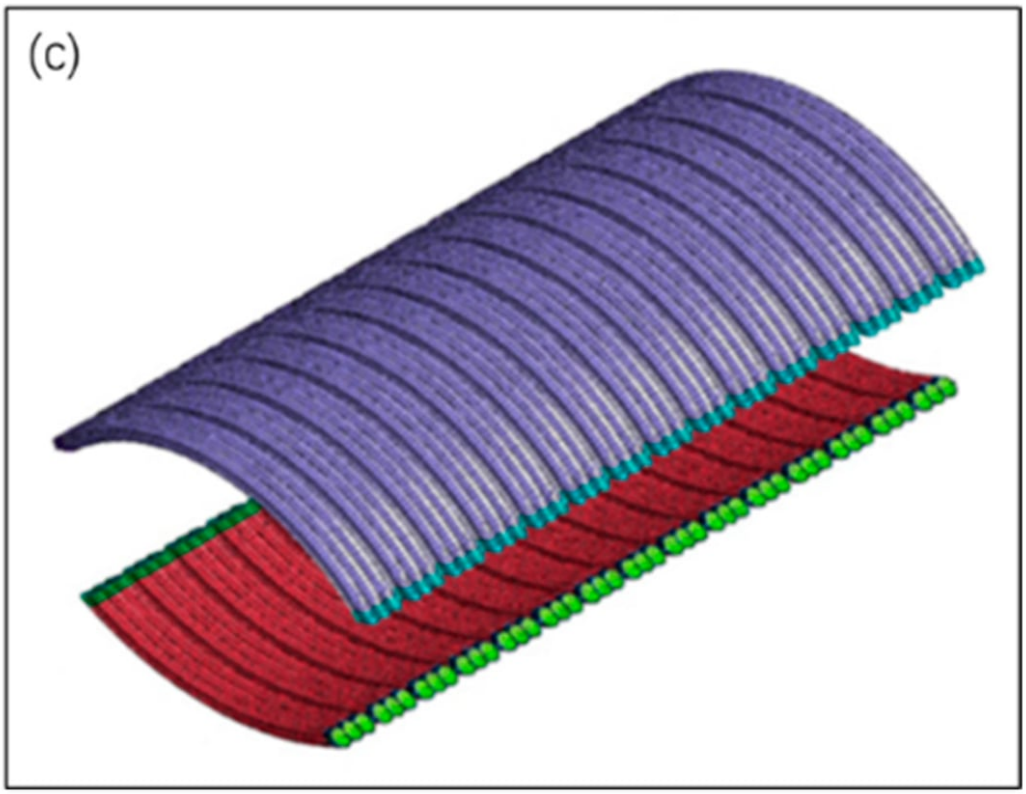


Figure 7. Numerical Model (m) (**a**) 3D ground-structure numerical model (**b**) Global tunnel model (**c**) Circumferential pipe curtain model.

Table 1. Physical and mechanical parameters of the strata.

	Elastic Modulus E (MPa)	Poisson's Ratio μ	Natural Unit Weight γ (kN/m^3)	Internal Friction Angle φ (°)	Cohesion c (kPa)
Soil layer 1	12	0.25	19.9	18.4	16.7
Soil layer 2	22	0.26	20.1	23.5	33.6
Soil layer 3	23	0.25	20.2	24.8	33.7

Note: The soil parameters were selected with reference to the project geotechnical investigation and the corresponding recommended design values.

Table 2. Material properties of the structural components.

Component	Material	Unit Weight γ (kN/m^3)	Elastic Modulus E (GPa)	Poisson's Ratio μ
Pipe curtain	Q355	78	210	0.30
Tunnel segment	C50	25	34.5	0.24
In-filled concrete	C50	25	34.5	0.24
Column	C50	25	34.5	0.24
Secondary lining	C40	25	31.5	0.30

The checked pipe-curtain–segment and beam-column connections use shared grid-points between adjoining continuum regions. This enforces displacement compatibility and

transfers load through the continuous mesh under an intact-connection assumption. No separate interface stiffness or friction parameters are assigned. According to the Chinese Code for Design of Concrete Structures (GB 50010) [31], the design values of tensile strength for C50 and C40 concrete are 1.89 MPa and 1.71 MPa, respectively. These parameters are used to identify vulnerable sections of the station and running tunnel, providing practical references for the construction process.

4. Result Analysis

The analysis follows the eight construction steps defined in Section 2.3 and Figure 6. Excavation, segment removal, structural activation, and temporary-support removal change the support configuration and redistribute loads among the ground and structural components.

Positive principal stress denotes tension, while negative principal stress denotes compression. Vertical displacement is positive upward and negative downward. Surface settlement is described below as a positive downward magnitude. The stress-contour legends indicate volumetric averaging; stress and displacement values are discussed in MPa and mm, respectively.

Local stresses are interpreted under the shared-gridpoint, intact-connection assumption described in Section 3. In the concrete regions, positive maximum principal stress is compared with the grade-specific tensile-strength reference to identify elevated local tensile demand. This comparison guides detailed connection assessment; it does not establish the capacity of a complete reinforced joint or simulate cracking.

4.1. Analysis of Surface Settlement Characteristics

The mid-section of the model along the Y-Z plane is selected as the monitoring section, with its center defined as the origin. Ground surface monitoring points are deployed at 10 m intervals within the range of −80 m to 80 m. The layout of these monitoring points is shown in Figure 8.

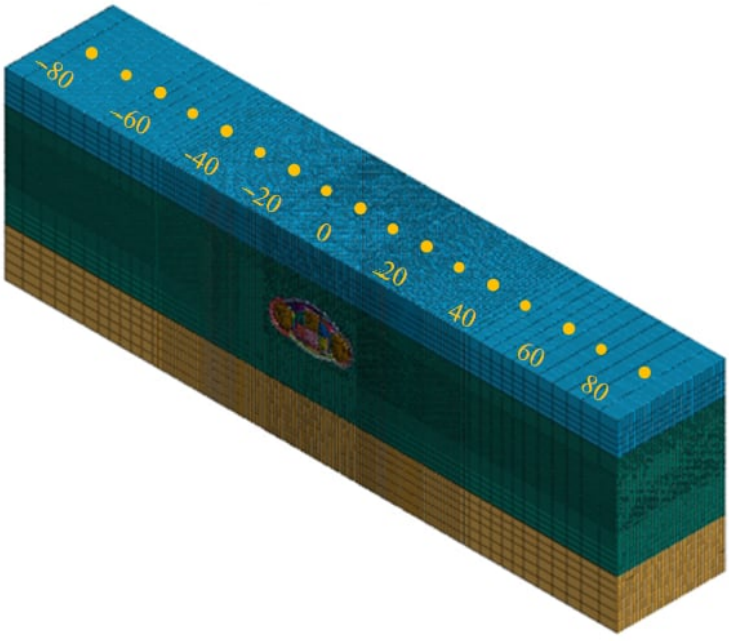


Figure 8. Layout of monitoring points.

The surface settlement curves are presented in Figure 9. The following observations can be drawn from these curves:

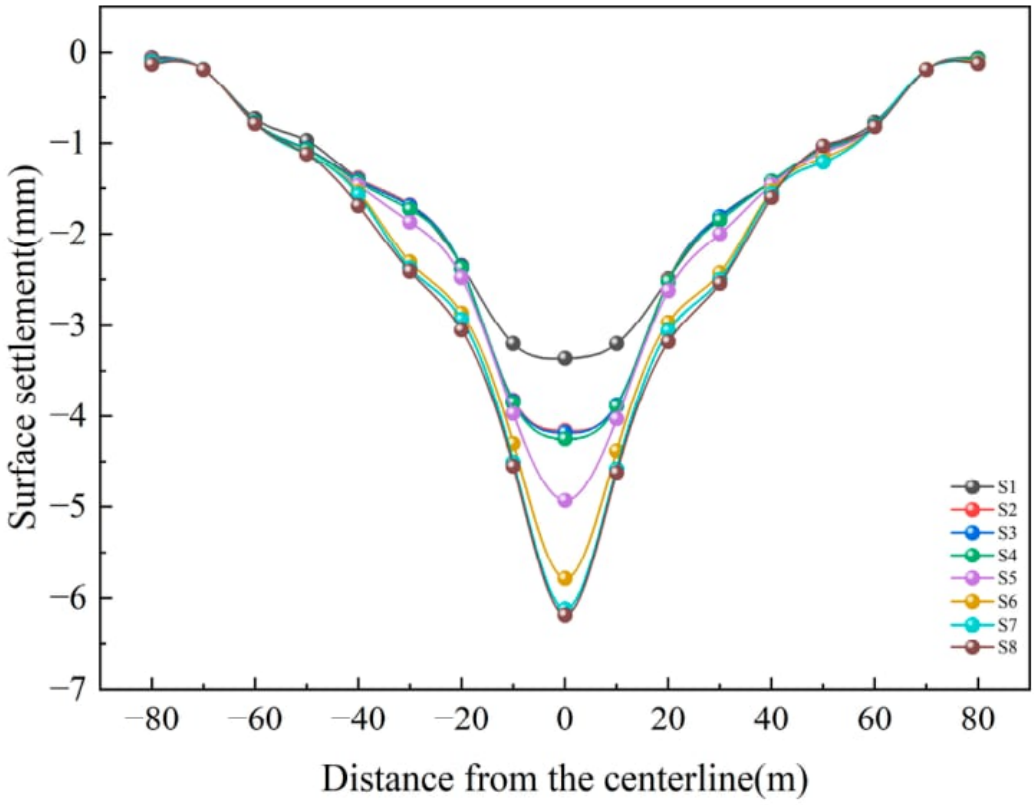


Figure 9. Surface displacement profiles at S1–S8. Negative plotted values denote downward movement.

(1) Maximum surface settlement occurs at the center line of the station and gradually decreases towards the edges. Noticeable settlement is concentrated within a range of 50 m from the center line. At the center line, the initial shield breakthrough induces a settlement of 3.36 mm. Subsequent construction operations add a further 2.82 mm to this value, resulting in a final maximum settlement of 6.18 mm.

(2) The surface settlement evolution throughout the construction process can be distinctly divided into three stages based on the construction steps. During the first stage, pipe curtain jacking alters the initial stress state of the soil mass. Consequently, surface settlement increases from 3.36 mm to 4.16 mm, initiating settlement accumulation at the station center line.

(3) The second stage corresponds to the transition period of the station support structure. Settlement continues to increase due to multiple localised construction activities. During this stage, the tunnel segments at the column locations are dismantled first, followed by the construction of the beams and columns. The alteration of local constraints causes stress redistribution, raising the settlement to 4.93 mm and expanding its influence zone. Subsequently, the large cross-section of the station is excavated. The underlying soil mass deforms due to the loss of confinement, which further increases the settlement to 5.79 mm. Next, the remaining tunnel segments are dismantled. The surrounding earth pressure previously borne by these segments is released, altering the load transfer path and causing the settlement at the station center to increase to 6.12 mm.

(4) The third stage covers permanent-lining installation and temporary-support removal. These operations change the structural configuration and redistribute loads. During this period, surface settlement increases only slightly, from 6.15 mm to 6.18 mm. This

small increment characterizes the response toward the end of the simulated construction sequence, while the preceding settlement increases remain relevant to construction-stage assessment.

(5) During station enlargement, S5 and S6 produce settlement increments of 0.86 mm and 0.33 mm, respectively. These operations warrant particular attention when coordinating excavation, segment removal, support installation, and deformation monitoring.

4.2. Mechanical Response Analysis of the Circumferential Pipe Curtain

4.2.1. Stress Characteristics of the Circumferential Pipe Curtain

The distributions of the maximum principal stress for the circumferential pipe curtain at various stages are shown in Figure 10. A comparison of their peak values is shown in Figure 11. The following observations can be made:

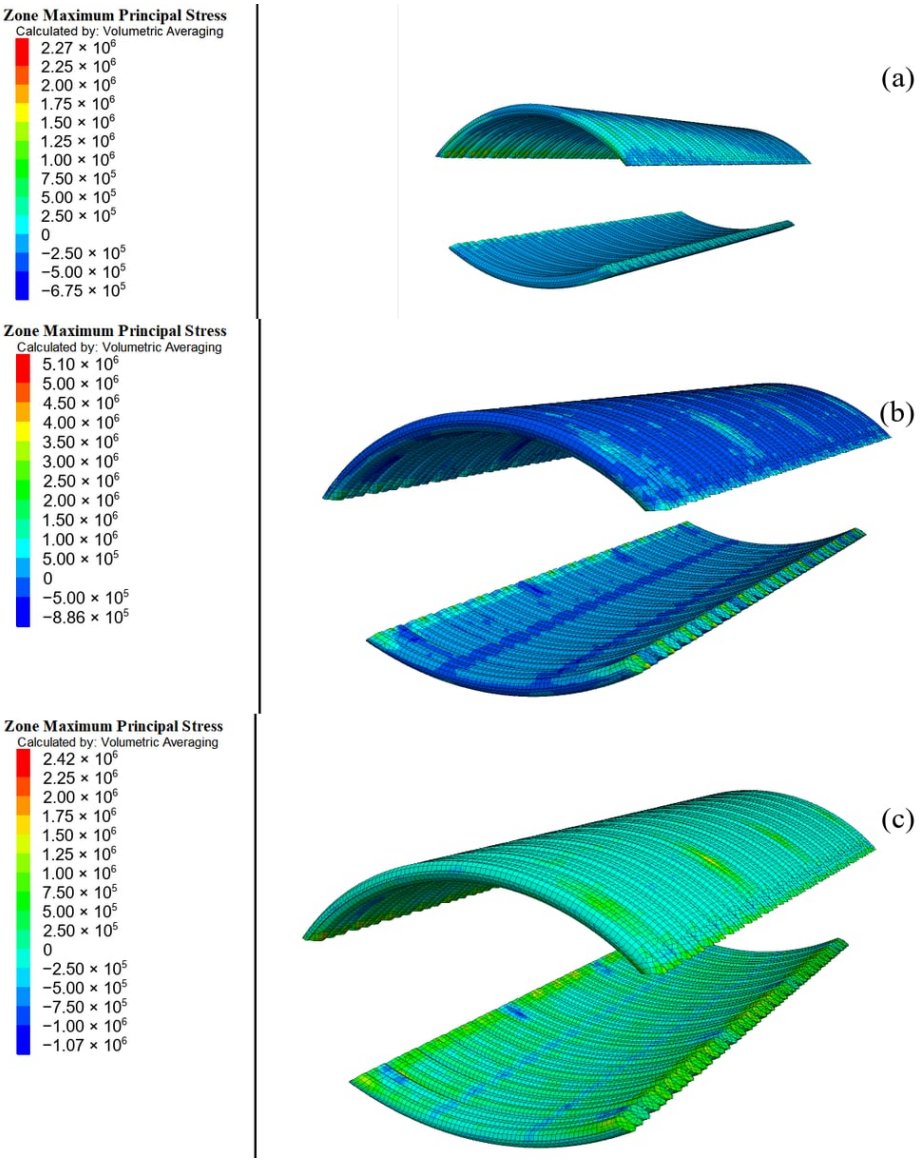


Figure 10. Maximum principal stress contours of the pipe curtains at (**a**) S3, (**b**) S6, and (**c**) S8, as defined in Figure 6. Stress is shown in Pa, with negative values denoting compression and positive values denoting tension.

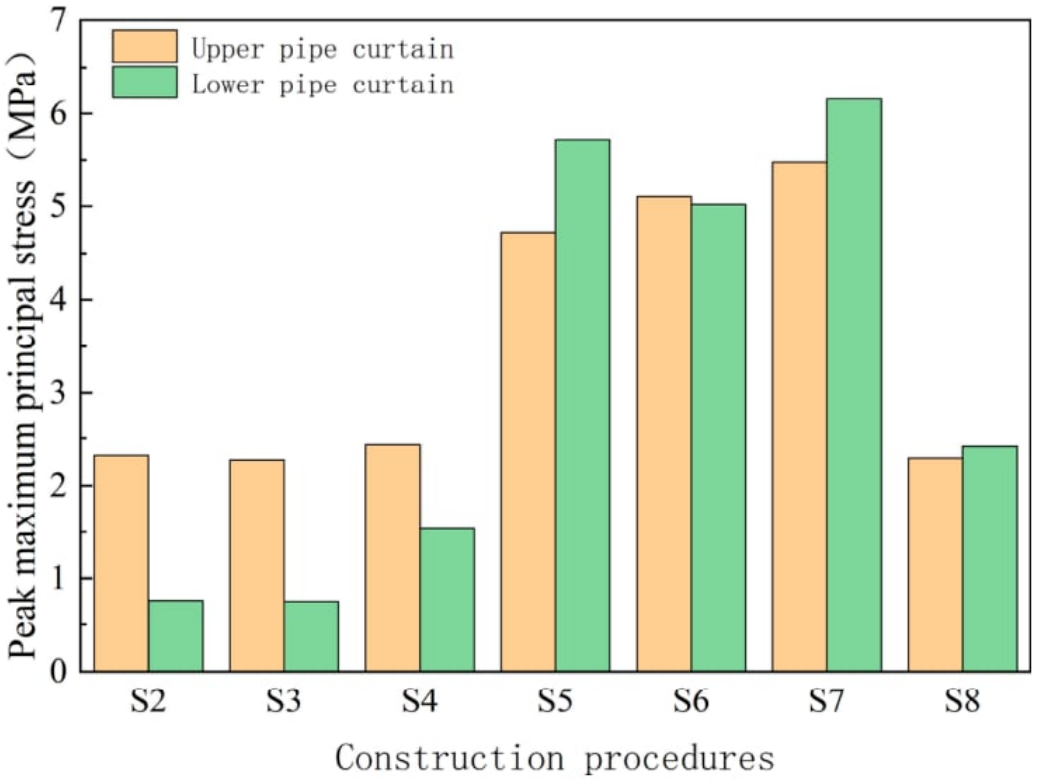


Figure 11. Peak maximum principal stress of the pipe curtain.

(1) Throughout the entire construction process, the maximum principal stress distribution of the pipe curtain exhibits systematic variations. It generally exhibits smaller early changes, increased tensile demand during structural-system transition, and a later reduction in the reported peak values. During this process, the joint region between the pipe curtain and the tunnel segments consistently remains a stress concentration zone. As construction progresses, this zone gradually expands towards the outer side of the pipe curtain at the column locations.

(2) In the first stage, the pipe curtain remains in an initial equilibrium state. During the transition of the force system in the second stage, the stress increases significantly. Dismantling the tunnel segments at the columns increases the maximum principal stresses of the upper and lower pipe curtains to 2.43 MPa and 1.54 MPa, respectively. Subsequently, the station expansion excavation releases the confinement of the soil mass, causing their peak values to surge to 4.72 MPa and 5.72 MPa, respectively. After removing the remaining tunnel segments, the load-bearing mechanism transitions to a collaborative load-bearing state between the pipe curtain and the beam-column system.

(3) During the system transition in the third stage, installing the longitudinal beams and the station secondary lining increases the upper and lower peak values to 5.48 MPa and 6.16 MPa, respectively. Further lining installation and temporary-support removal modify the load paths and redistribute local stress demand. The upper and lower peak stresses subsequently decrease to approximately 2.29 MPa and 2.42 MPa, respectively. The preceding tensile peaks at S7 identify the pipe-curtain connections as priorities for construction-stage assessment.

The distributions of the minimum principal stress for the circumferential pipe curtain at various stages are shown in Figure 12. A comparison of their peak values is shown in Figure 13. The following observations can be made:

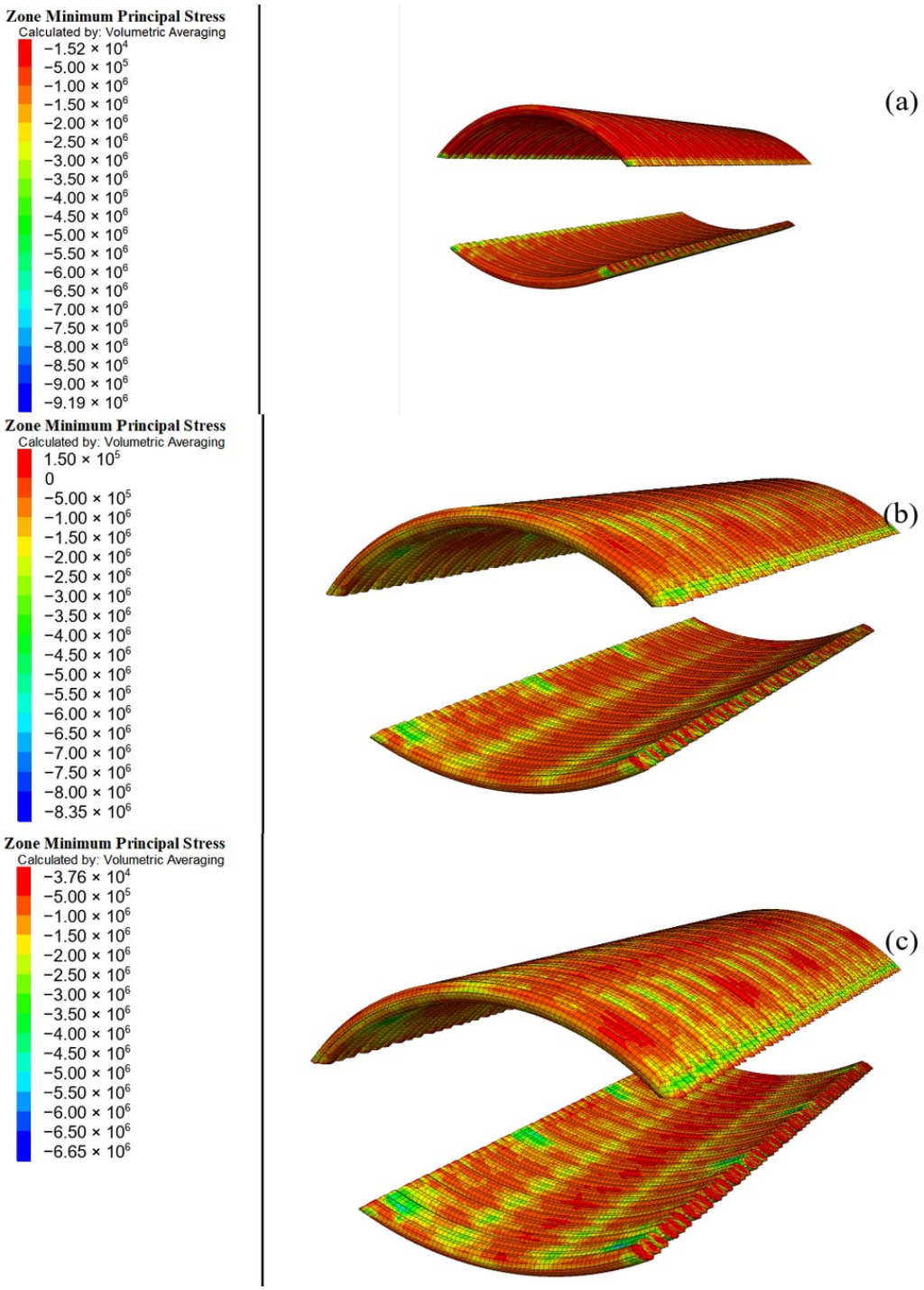


Figure 12. Minimum principal stress contours of the pipe curtains at (**a**) S3, (**b**) S6, and (**c**) S8, as defined in Figure 6. Stress is shown in Pa, with negative values denoting compression and positive values denoting tension.

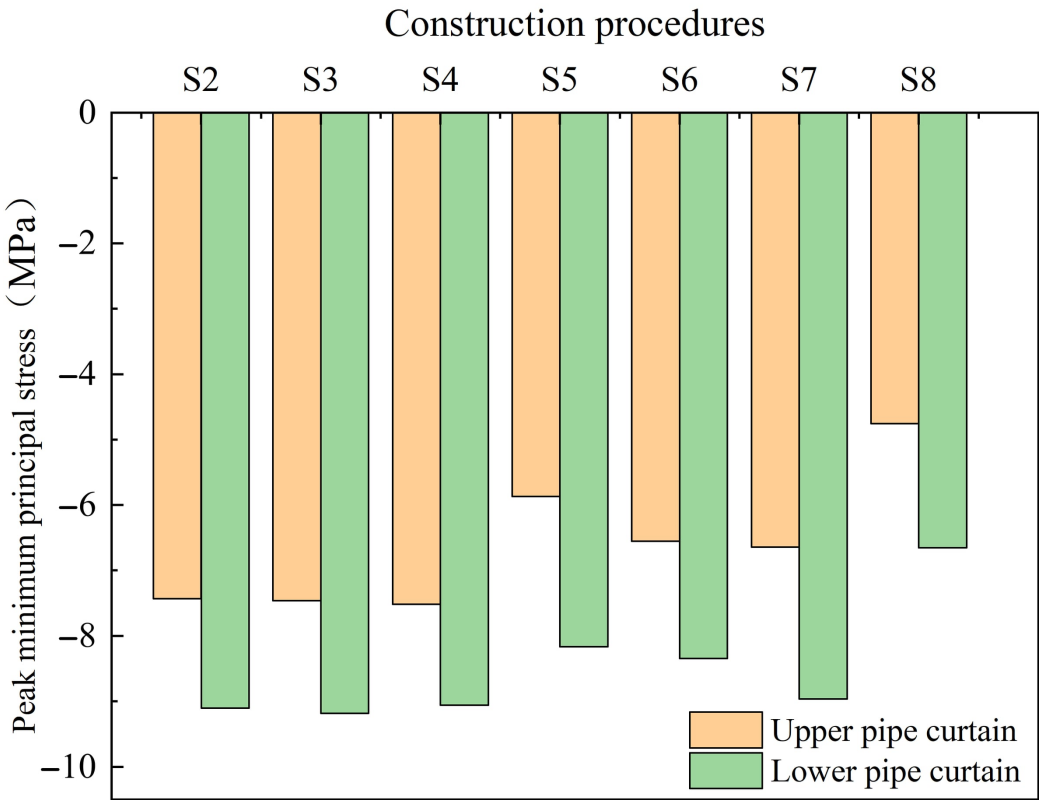


Figure 13. Peak minimum principal stress of the pipe curtain.

(1) Throughout the entire construction process, the minimum principal stress distribution of the pipe curtain exhibits systematic characteristics. It generally exhibits early compressive demand, fluctuations during structural-system transition, and a later reduction in compressive magnitude. This indicates redistribution of local compressive demand as the support configuration changes. The lower-curtain contour minimum is approximately −9.19 MPa at S3, while the upper curtain reaches approximately −7.52 MPa at S4. The controlling steps for compression therefore differ from those for tension.

(2) In the first stage, the pipe curtain remains in an initial equilibrium state. During the transition of the force system in the second stage, the stress fluctuates and adjusts. Dismantling the tunnel segments at the columns and constructing the beam columns causes stress redistribution. Consequently, the peak minimum principal stresses of the upper and lower pipe curtains become −7.52 MPa and −9.06 MPa, respectively. Station expansion excavation changes soil confinement and the restraint around the pipe curtain. The compressive magnitudes then decrease, with values of −5.87 MPa and −8.17 MPa for the upper and lower curtains, respectively. After removing the remaining tunnel segments, the stress distribution range expands, and the peak values rebound to −6.55 MPa and −8.35 MPa.

(3) In the third stage, installation of the longitudinal beams and station secondary lining changes the structural configuration, with the upper and lower minimum principal stresses reaching −6.65 MPa and −8.96 MPa, respectively. Subsequent temporary-support removal and lining installation further redistribute local stresses. The corresponding values become −4.76 MPa and −6.65 MPa at S8, indicating reduced compressive magnitudes toward the end of the simulated sequence.

4.2.2. Deformation Characteristics of the Circumferential Pipe Curtain

Figure 14 illustrates the Z-direction displacement distribution of the circumferential pipe curtain across various stages, while Figure 15 presents a comparison of their peak values. The following observations can be made:

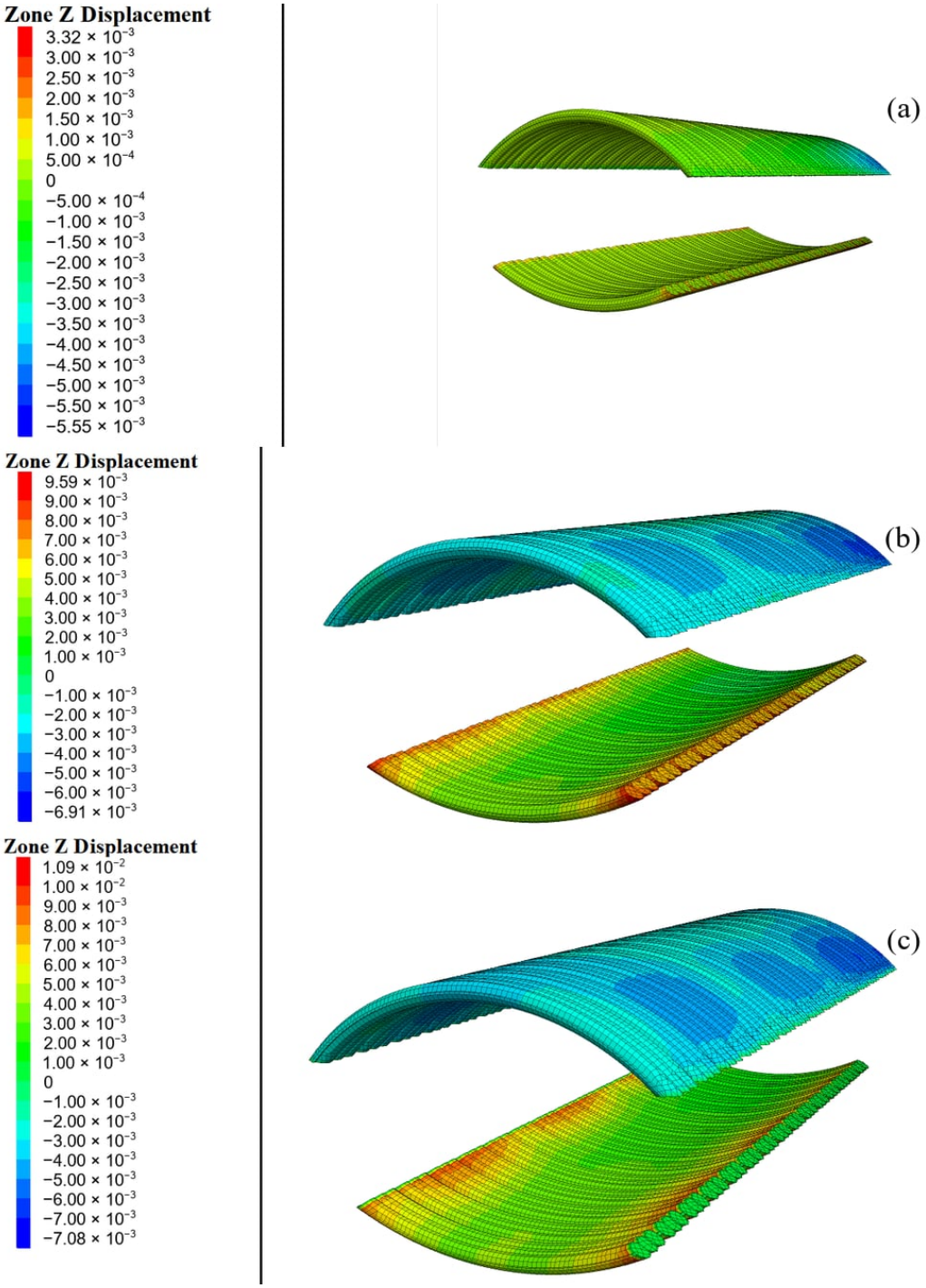


Figure 14. Z-direction displacement contours of the pipe curtains at (**a**) S3, (**b**) S6, and (**c**) S8, as defined in Figure 6. Displacement is shown in m, with positive values denoting heave and negative values denoting settlement.

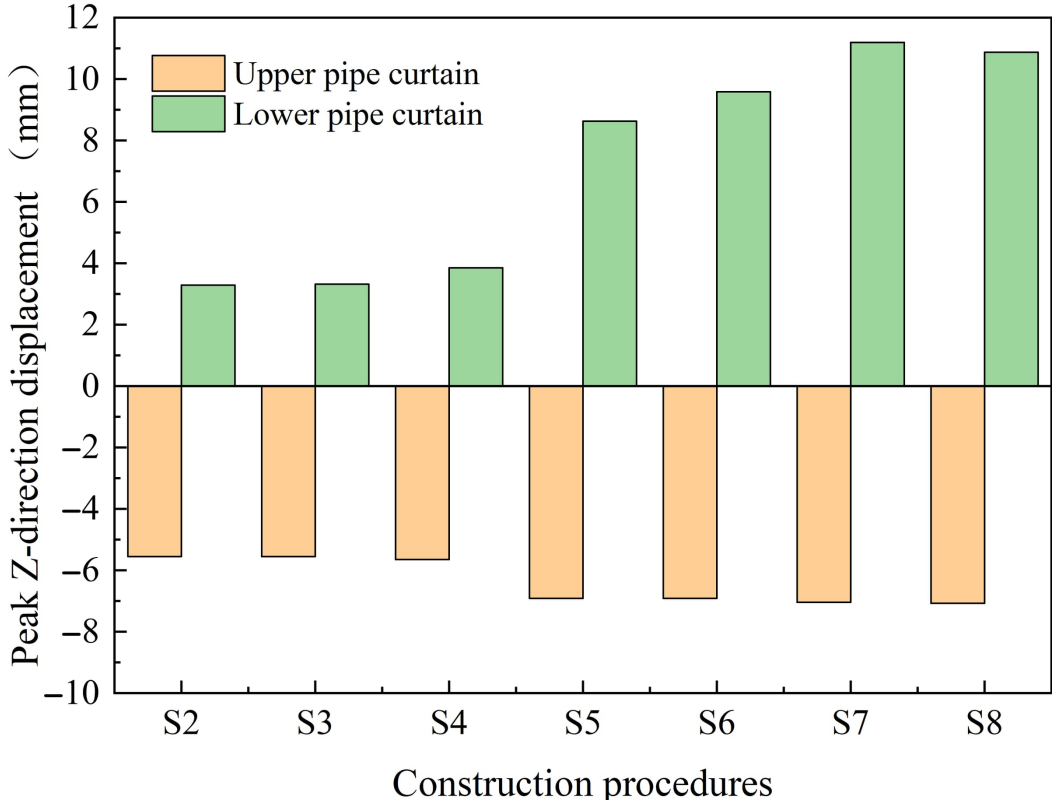


Figure 15. Peak Z-direction displacement of the pipe curtain.

(1) Throughout the construction process, the Z-direction displacement of the pipe curtain exhibits a clear evolution: an initial equilibrium, followed by a sharp increase, and eventual stabilization. The displacement is initially concentrated at the joints between the pipe curtain and the tunnel segments. As construction advances, it gradually expands to the upper pipe curtain between adjacent columns.

(2) During the first construction stage, the pipe curtain remains in an initial equilibrium state. Upon entering the second stage, its deformation significantly increases and redistributes. First, removing the tunnel segments at the columns and constructing the beam-column system alter the local boundary conditions. This increases the Z-direction displacement around the joints between the pipe curtain and the segments, with the peak displacements of the upper and lower pipe curtains reaching −5.65 mm and 3.85 mm, respectively.

The deformation increment of the lower pipe curtain is notably larger than that of the upper pipe curtain, indicating different responses to the changes in support conditions. Subsequent station expansion excavation reduces soil confinement around the pipe curtain. With the resulting changes in confinement and structural support, the upper and lower displacement extrema reach −6.91 mm and +8.63 mm, respectively.

At this point, the lower pipe curtain has the larger displacement magnitude, while large downward movements also occur in the upper curtain between adjacent columns. Finally, after removing the remaining tunnel segments, the larger displacements of the upper pipe curtain are primarily distributed along its outer side between the columns. Meanwhile, the lower pipe curtain's maximum displacement remains concentrated at the joints, further increasing to 9.59 mm.

(3) During the third stage, the top and bottom longitudinal beams and the station secondary lining are constructed. Activation of these structural regions changes the mod-

eled stiffness and self-weight loading. The lower-curtain heave consequently increases to 11.20 mm at S7, while the upper-curtain displacement reaches −7.04 mm.

Finally, temporary-support removal and completion of the tunnel secondary lining change the structural configuration and provide additional load paths.

At S8, the upper-curtain displacement reaches its reported maximum downward magnitude of −7.08 mm, while lower-curtain heave decreases to 10.88 mm. Thus, upper-curtain downward displacement is controlled by S8, whereas lower-curtain heave is greatest at S7. These different displacement histories support separate construction-stage checks for the upper and lower curtains.

4.3. Mechanical Response Analysis of the Tunnel Segments

4.3.1. Stress Characteristics of the Tunnel Segments

Figure 16 illustrates the maximum principal stress distribution of the tunnel segments across various stages, while Figure 17 compares the peak values. The following observations can be made:

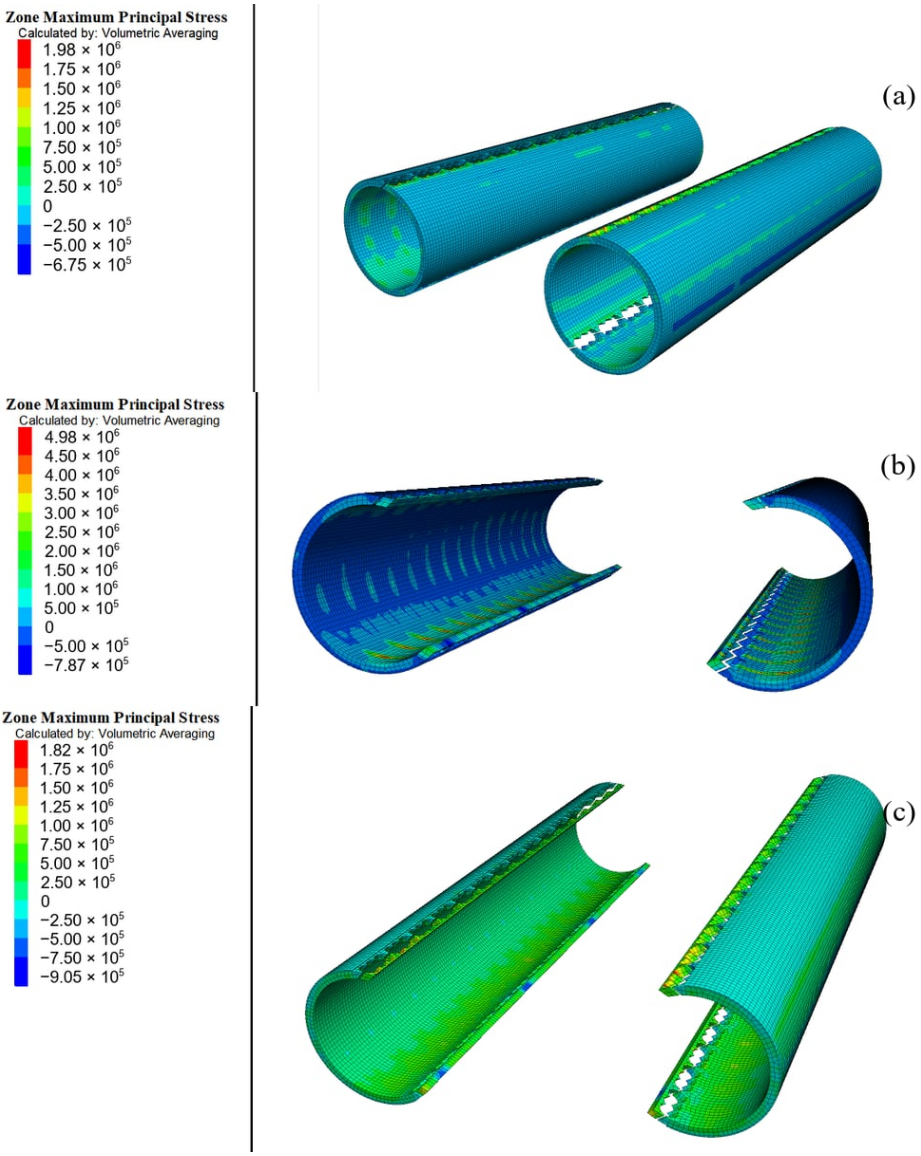


Figure 16. Maximum principal stress contours of the tunnel segments at (**a**) S3, (**b**) S6, and (**c**) S8, as defined in Figure 6. Stress is shown in Pa, with negative values denoting compression and positive values denoting tension.

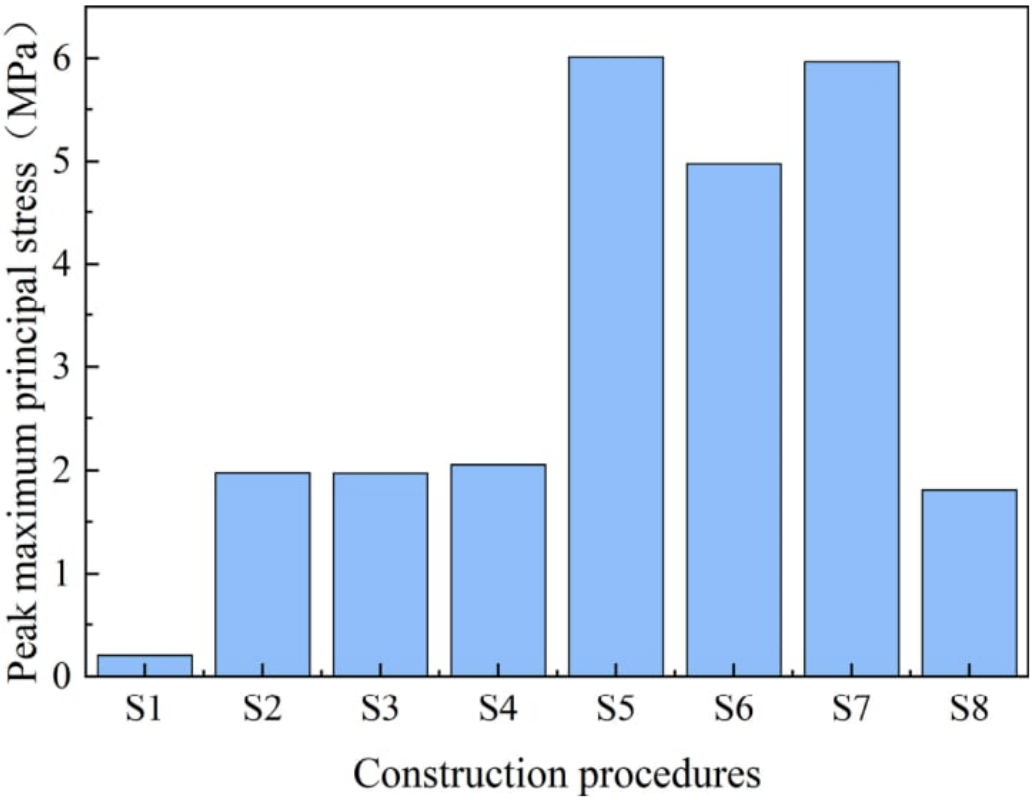


Figure 17. Peak maximum principal stress of the tunnel segments.

(1) Throughout the construction process, the maximum principal stress of the segments exhibits an evolution pattern of initial equilibrium, a sharp increase, and a subsequent decrease. The stress concentration zones consistently remain at the segment-pipe curtain joints and gradually expand to the contact areas of the temporary supports.

(2) During the first stage, the reported maximum principal stress reaches approximately +1.97 MPa, indicating local tensile demand under the adopted sign convention. In the second stage, the structural system transformation triggers dramatic stress fluctuations. Initially, removing local segments causes the peak stress to rise to 2.06 MPa. Subsequently, the station expansion excavation causes the stress at the joints between the segments and the lower pipe curtain to surge to 6.02 MPa. This value exceeds the adopted C50 concrete tensile-strength reference of 1.89 MPa and identifies elevated local tensile demand. The corresponding connection regions are therefore identified for detailed reinforcement and anchorage assessment and construction-stage monitoring.

Finally, after removing the remaining segments, the resulting load transfer reduces the peak stress to 4.98 MPa. At this point, the stress concentrates primarily at the contact areas of the temporary supports.

(3) In the early phase of the third stage, the construction of the longitudinal beams and secondary lining transfers the dead weight, causing the stress to rise back to 5.97 MPa. Following further lining installation and temporary-support removal, the maximum principal stress decreases to 1.82 MPa at S8. The remaining positive value indicates residual local tensile demand.

The segment–pipe-curtain connections and temporary-support contact regions should therefore remain key targets for construction-stage monitoring and detailed connection assessment.

Figure 18 illustrates the minimum principal stress distribution of the tunnel segments across various stages, while Figure 19 compares the peak values. The following observations can be made:

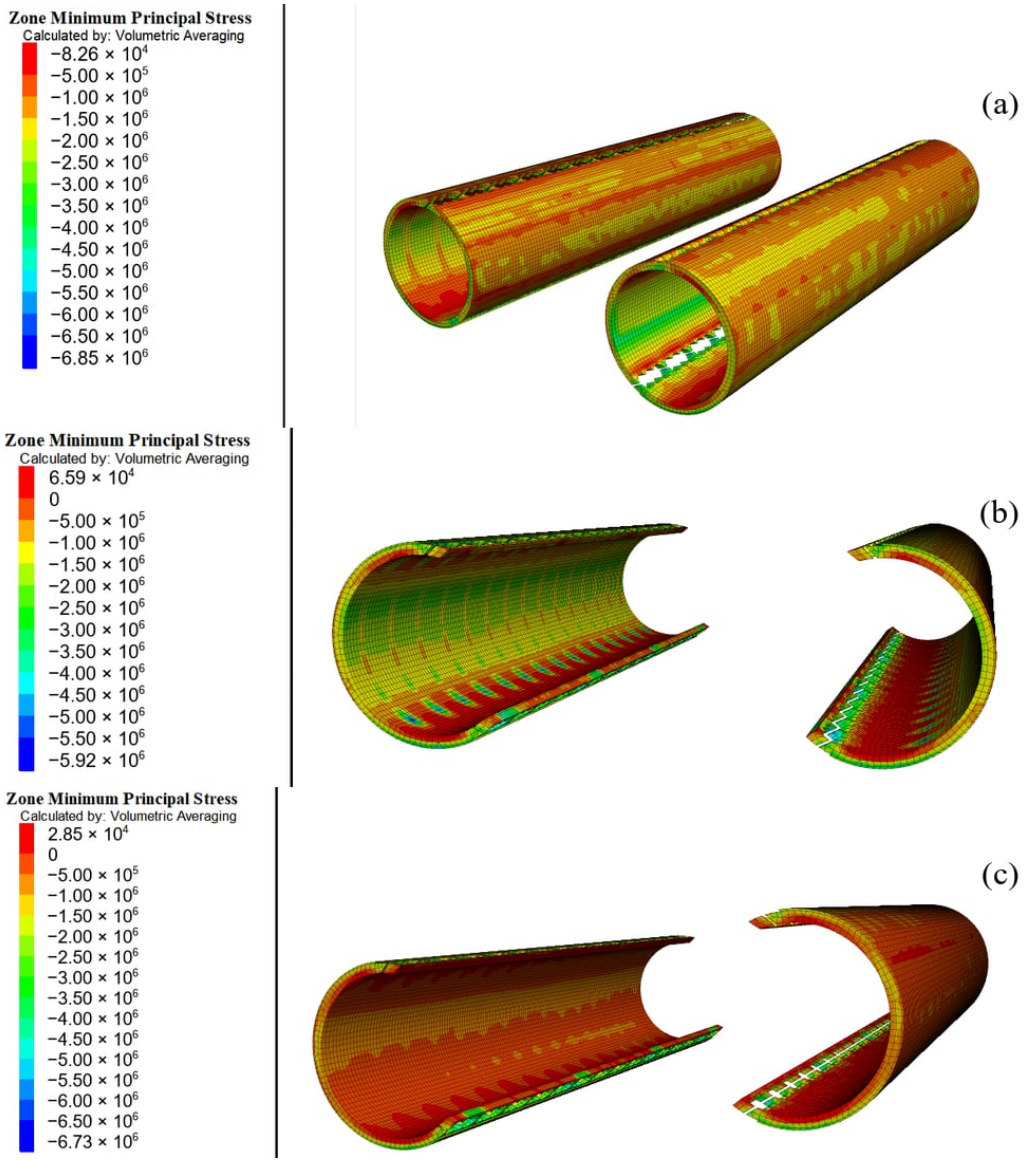


Figure 18. Minimum principal stress contours of the tunnel segments at (**a**) S3, (**b**) S6, and (**c**) S8, as defined in Figure 6. Stress is shown in Pa, with negative values denoting compression and positive values denoting tension.

(1) Throughout the construction process, the minimum principal stress of the segments exhibits a clear evolution pattern: initial equilibrium, subsequent fluctuation, and eventual stabilization. The compressive stress concentration zones gradually shift from the invert and adjacent haunches to the segment-pipe curtain joints.

(2) During shield breakthrough, the segment response contains compressive regions. At this point, the peak minimum principal stress is −4.52 MPa. After the pipe curtain jacking, the compressive stress at the joints sharply increases to −6.83 MPa.

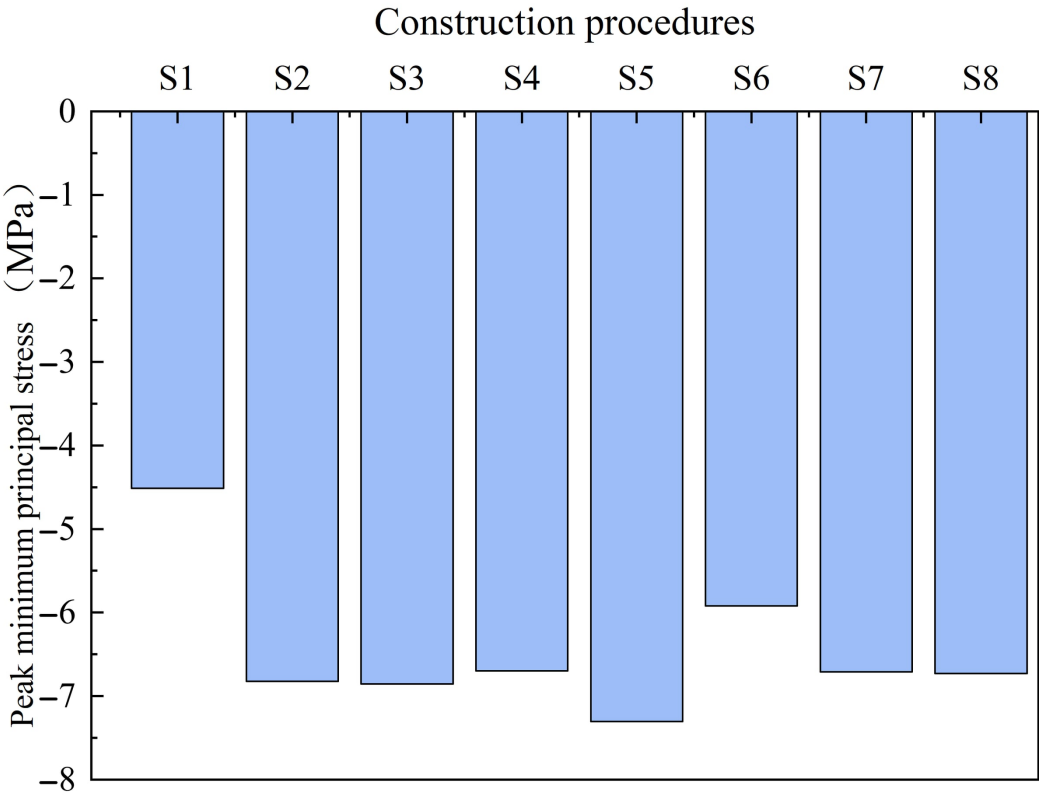


Figure 19. Peak minimum principal stress of the tunnel segments.

In the second stage, the structural system transformation triggers stress fluctuations. Removing the tunnel segments at the columns causes the compressive stress to drop slightly to −6.70 MPa. Subsequently, the station expansion excavation increases the stress at the haunches to −7.31 MPa. Finally, removing the remaining segments produces further stress redistribution. This reduces the peak value to −5.92 MPa, concentrating it at the temporary support contact surfaces in the invert.

(3) During the third stage, lining activation and temporary-support removal change the segment support conditions. The reported final minimum principal stress is −6.73 MPa. The compression concentrations at the segment–pipe-curtain connections are considered alongside the residual local tensile demand reported above, providing references for selecting locations for detailed connection assessment.

4.3.2. Deformation Characteristics of the Tunnel Segments

Figure 20 illustrates the Z-direction displacement distribution of the shield tunnel segments across various construction stages, while Figure 21 compares their peak values. The following observations can be made:

(1) Throughout the construction process, the Z-direction displacement concentration zones of the segments consistently remain at the crown and invert on the adjacent sides of the two tunnels. The overall displacement evolution undergoes three distinct phases: smaller early movements, increased displacement during structural-system transition, and smaller late-stage changes. During the first stage, segment deformation develops rapidly alongside the jacking of the circumferential pipe curtain. The crown settlement increases to 11.40 mm, while the invert heave reaches 7.10 mm. At this stage, crown settlement dominates the overall deformation.

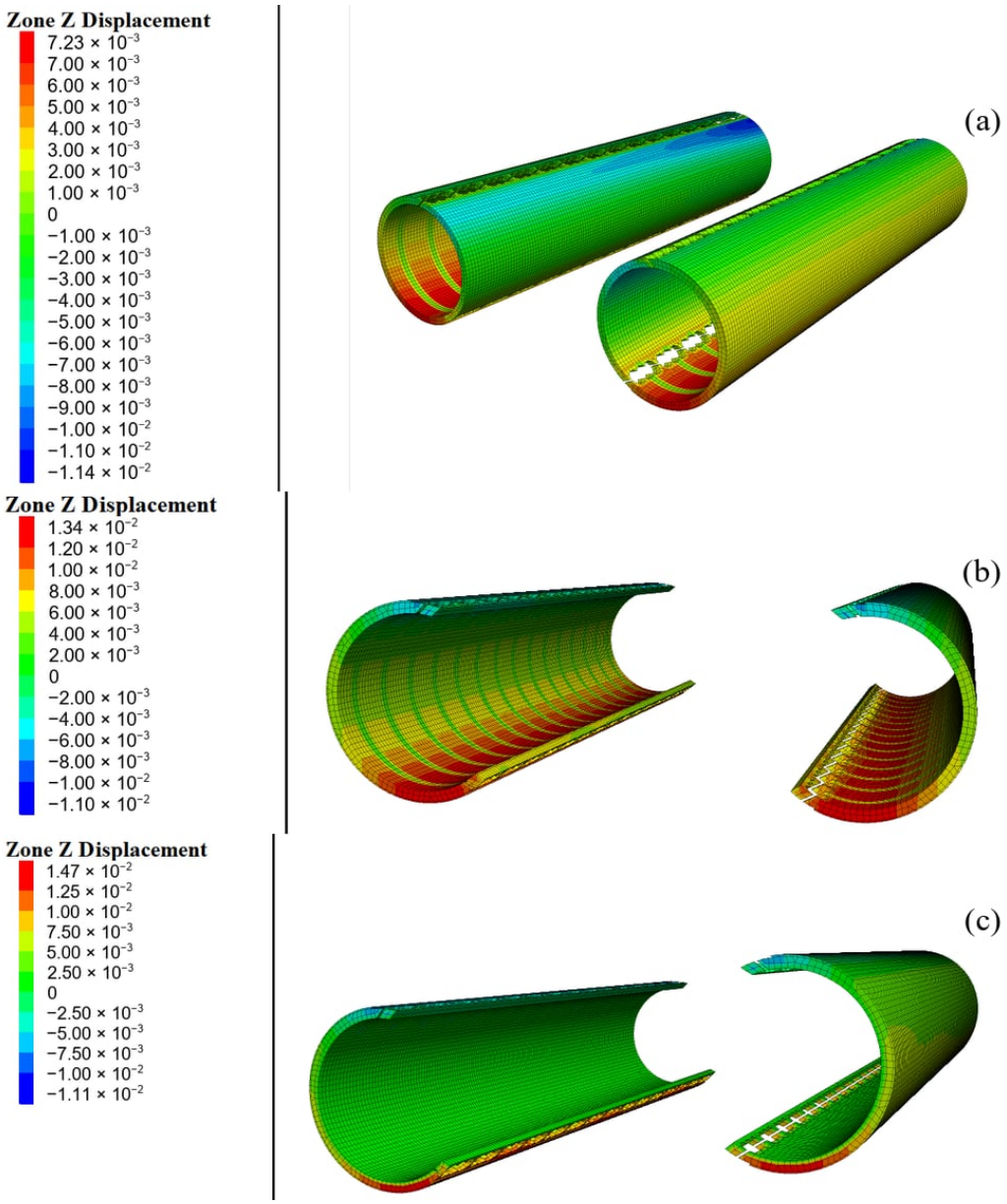


Figure 20. Z-direction displacement contours of the tunnel segments at (**a**) S3, (**b**) S6, and (**c**) S8, as defined in Figure 6. Displacement is shown in m, with positive values denoting heave and negative values denoting settlement.

(2) During the structural system transformation in the second stage, segment deformation gradually increases in steps. Notably, the invert heave increases much more significantly than the crown settlement. First, removing the segments at the columns and constructing the beam-column system alter the local boundary conditions. The newly formed local support from the beams and columns reduces the crown settlement to 10.99 mm.

Subsequently, the large-section expansion excavation of the station removes the surrounding soil support for the segments. This triggers a distinct basal rebound, causing the invert heave to surge to 12.54 mm. Consequently, the primary deformation location shifts downward from the crown. Next, removing the remaining segments reduces the overall structural stiffness. The crown settlement slightly drops to 10.98 mm, while the invert heave further increases to 13.45 mm. The structural stress state begins transitioning into a collaborative load-bearing system formed by the segments, pipe curtain, and beam-column system.

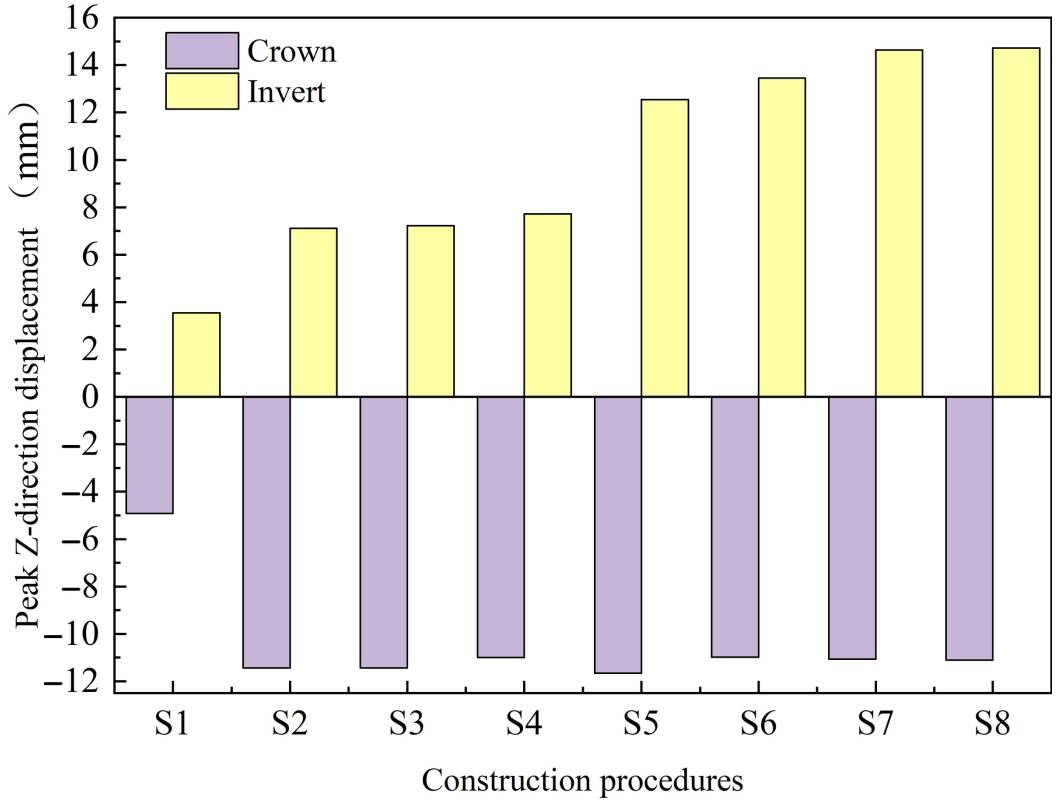


Figure 21. Peak Z-direction displacement of the tunnel segments.

(3) In the third stage, the top and bottom longitudinal beams and the secondary linings of both the running tunnel and the station are successively constructed and closed to form a ring. This finalizes the joint load-bearing system between the segments and the secondary lining. Following this, the reported displacement increments become smaller toward the end of the construction sequence.

The final calculated crown settlement is approximately 11.10 mm, while invert heave reaches 14.72 mm at S8. The dominant displacement magnitude therefore shifts from early crown settlement to later invert heave. This pattern identifies the invert and its nearby support-contact regions as priorities for construction-stage monitoring, alongside the crown.

4.4. Mechanical Response Characteristics of the Beam-Column System

4.4.1. Stress Characteristics of the Beam-Column System

Figure 22 illustrates the maximum principal stress distribution of the beams and columns across various stages, while Figure 23 compares the peak values. The S8 contours include the activated lining regions and are interpreted as displays of the assembled structural system. The following observations can be made:

(1) Throughout the construction process, the maximum principal stress of the beams and columns exhibits a pattern of initial stability, a sharp increase, and a subsequent decrease. The stress concentration zones gradually expand from the corbels of the top longitudinal beams at the columns to the bottom of the bottom longitudinal beams, and ultimately to the joints between the tunnel secondary lining and the pipe curtain.

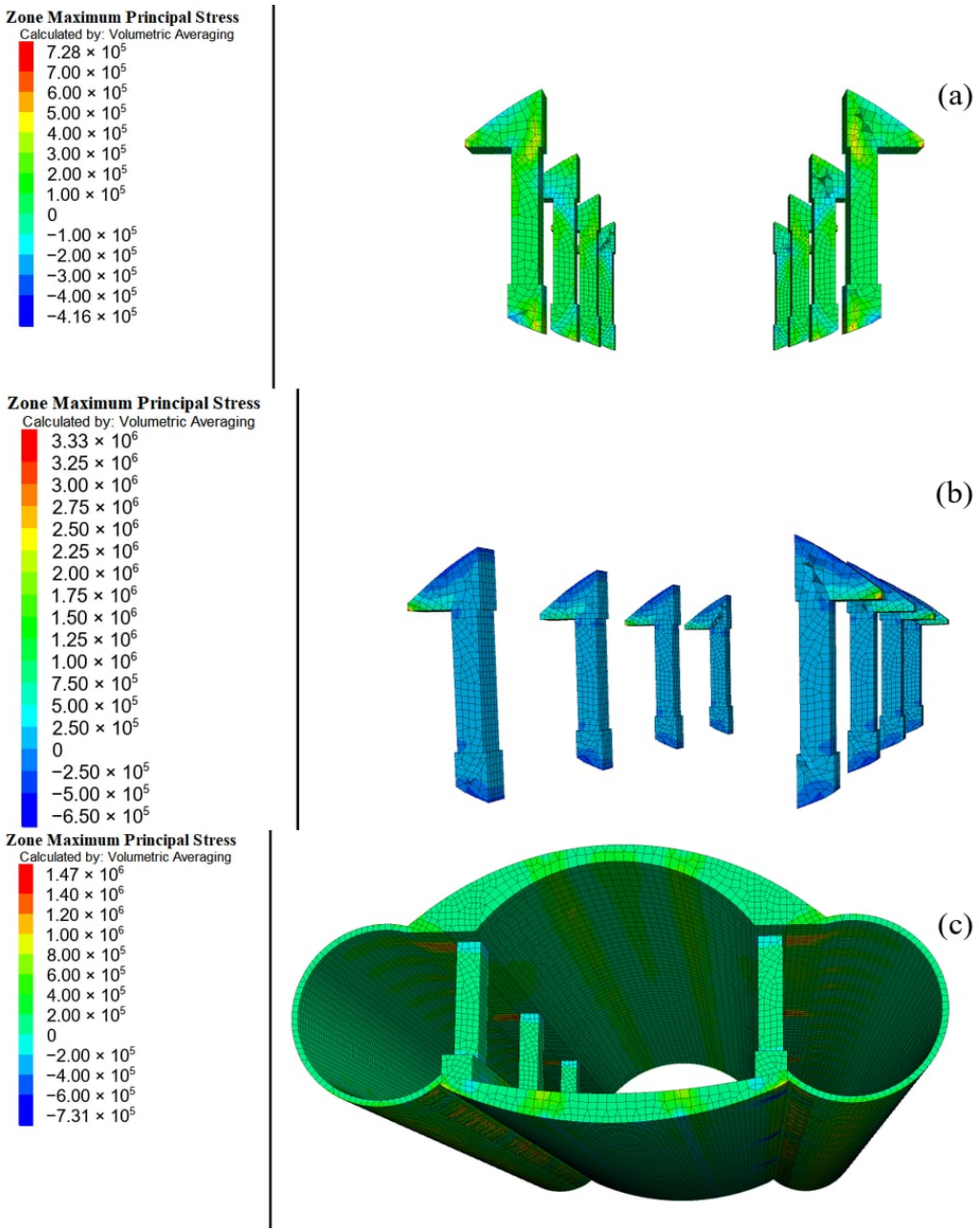


Figure 22. Maximum principal stress contours of beams and columns at (**a**) S4, (**b**) S6, and (**c**) S8, as defined in Figure 6. Stress is shown in Pa, with negative values denoting compression and positive values denoting tension.

(2) During the structural system transformation stage, removing the tunnel segments at the columns generates an initial stress of 0.73 MPa at the corbels of the top longitudinal beams. The station expansion excavation then forces the loads to transfer to the beams and columns, causing the stress at the corbels to surge to 2.13 MPa. Later, removing the remaining tunnel segments decreases the boundary support stiffness. Consequently, the corbel stress reaches 3.33 MPa at S6, exceeding the adopted C40 concrete tensile-strength reference of 1.71 MPa and identifying elevated local tensile demand during the removal of the remaining segments.

(3) Subsequently, constructing the longitudinal beams and the station secondary lining enhances the overall structural stiffness. This causes the maximum principal stress to decrease to 2.73 MPa and shift to the bottom of the longitudinal beams. Temporary-support removal and further lining installation modify the load paths of the assembled system.

The displayed maximum principal stress decreases to 1.47 MPa at S8, with a concentration near the secondary-lining–pipe-curtain connection. The upper longitudinal-beam corbels nevertheless remain priorities for detailed reinforcement, anchorage, and construction-stage monitoring, with S6 identified as the reported tensile-demand control step.

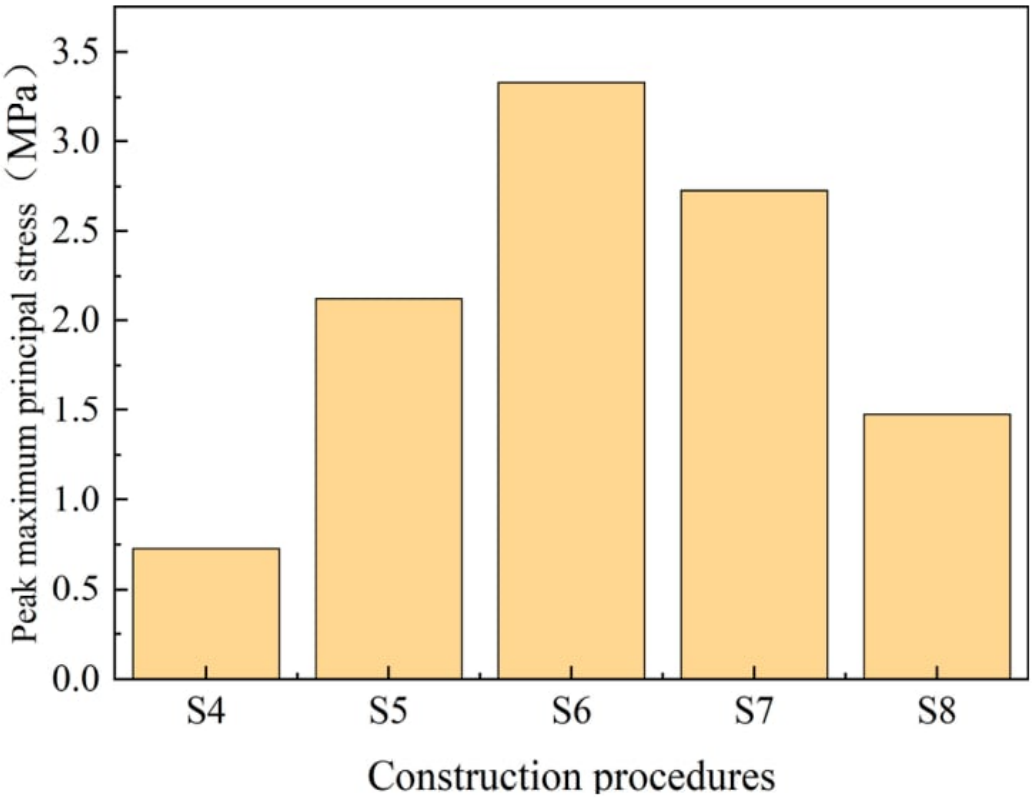


Figure 23. Peak maximum principal stress of the beams and columns.

Figure 24 illustrates the minimum principal stress distribution of the beams and columns across various stages, while Figure 25 compares the peak values. The following observations can be made:

(1) Throughout the construction process, the minimum principal stress of the beam-column structure exhibits an evolution pattern of initial stability, a sharp increase, and eventual stabilization. The compressive stress concentration zones consistently remain at the column-longitudinal beam joints and the bottom of the bottom longitudinal beams. As construction advances, these zones gradually expand from the column bases to the middle-lower sections of the columns.

(2) During the early phase of the structural system transformation, the tunnel segments at the columns are removed, and the beam-column system is constructed. At this stage, the beam-column regions are activated before station expansion excavation. Loads are transferred through the segment, pipe-curtain, temporary-support, and newly activated beam-column regions. The peak minimum principal stress remains at a low level of −3.63 MPa, concentrating at the bottom of the bottom longitudinal beam near the columns.

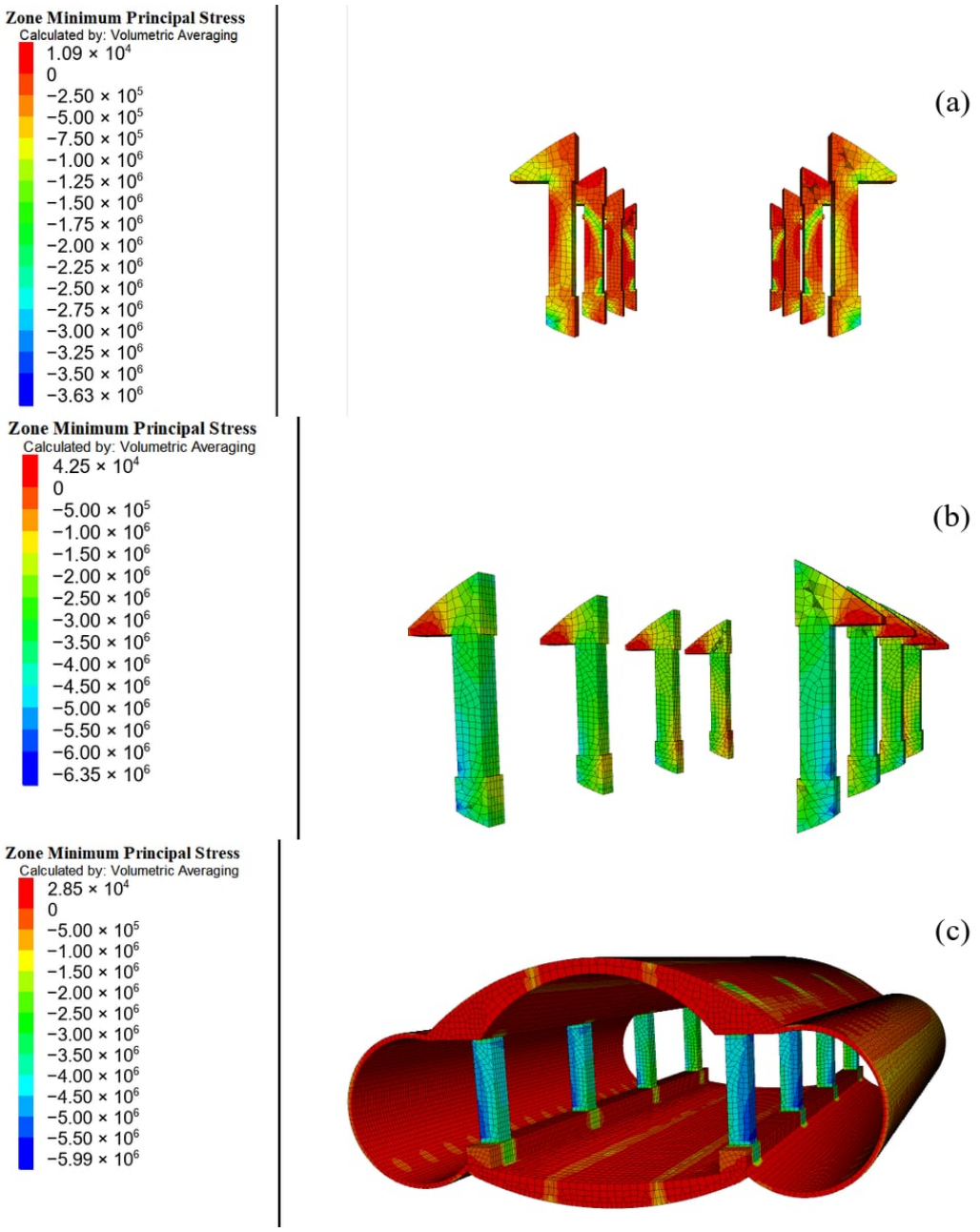


Figure 24. Minimum principal stress contours of the beams and columns at (**a**) S4, (**b**) S6, and (**c**) S8, as defined in Figure 6. Stress is shown in Pa, with negative values denoting compression and positive values denoting tension.

Upon entering the large-section expansion excavation stage, the radial soil constraint is removed, triggering stress redistribution. The beam-column system begins to bear the primary loads. Consequently, the peak minimum principal stress significantly increases to −5.89 MPa, and the concentration zone shifts to the joints between the columns and the longitudinal beams.

Subsequently, removing the remaining segments further weakens the segment support effect. Loads rapidly transfer through the columns to the bottom longitudinal beams. The peak minimum principal stress reaches a peak of −6.35 MPa, increasing the overall magnitude of compressive stress and shifting the stress concentration zone toward the column bases.

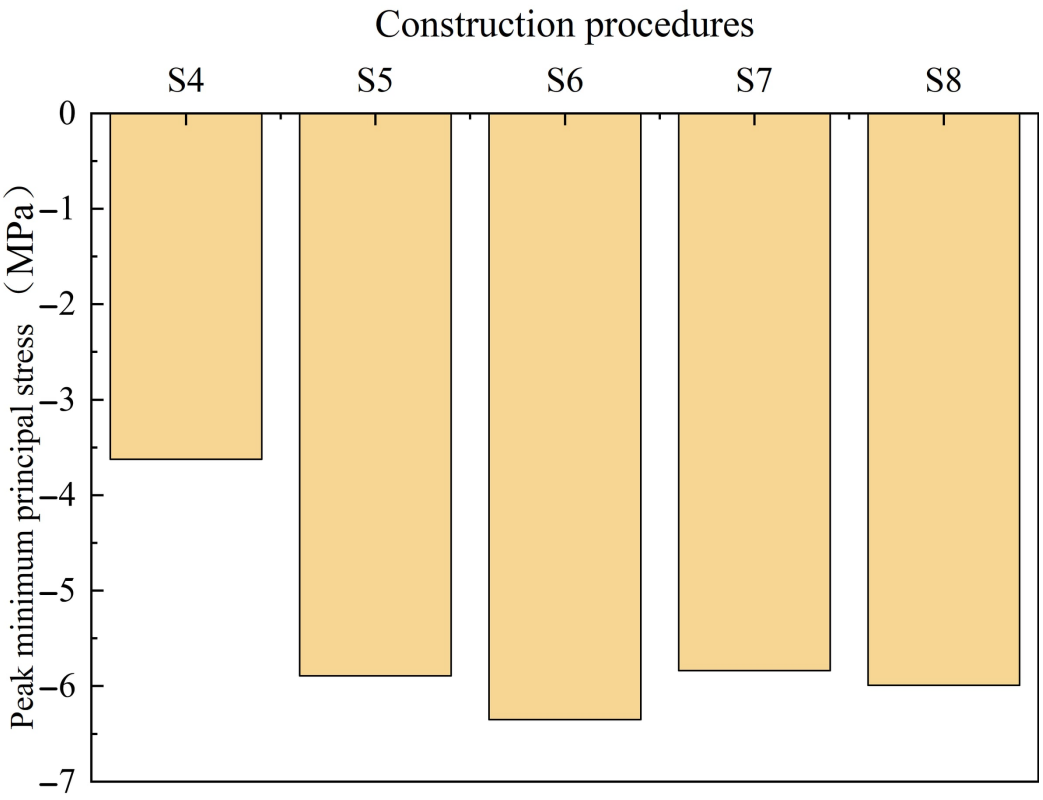


Figure 25. Peak minimum principal stress of the beams and columns.

(3) Finally, the secondary linings of both the station and the running tunnel successively close to form complete rings. These secondary linings combine with the beams and columns to form a composite frame structure that synergistically bears the stress. Thus, lining activation modifies the load paths through the assembled structural system.

At S8, the assembled-system contour gives a minimum principal stress of approximately −5.99 MPa. This final display is considered alongside the S6 compressive demand at the lower beam-column connections, which remains relevant to local bearing and load-transfer assessment.

4.4.2. Deformation Characteristics of the Beam-Column System

Figure 26 illustrates the Z-direction displacement distribution of the beams and columns across various stages. Meanwhile, Figure 27 presents a comparison of their peak values. The following observations can be made:

(1) Throughout the construction process, the Z-direction displacement of the beam-column structure exhibits a clear evolution pattern: initial stability, a significant increase, and eventual stabilization. The trapezoidal corbels at the joints between the top longitudinal beams and the columns consistently remain the deformation concentration zones. As construction advances, these zones gradually expand to the bottom longitudinal beams and the middle-lower sections of the columns.

During the early phase of the structural system transformation, segments at the columns are removed, and the beam-column system is constructed. At this stage, the newly established beam-column system relies primarily on the tunnel segments, the pipe curtain, and the temporary supports to jointly bear loads. Consequently, the displacements remain relatively small compared with the later steps. The upper longitudinal-beam–column joints and lower longitudinal beams exhibit vertical displacement extrema of approximately −0.59 mm and +0.55 mm, respectively.

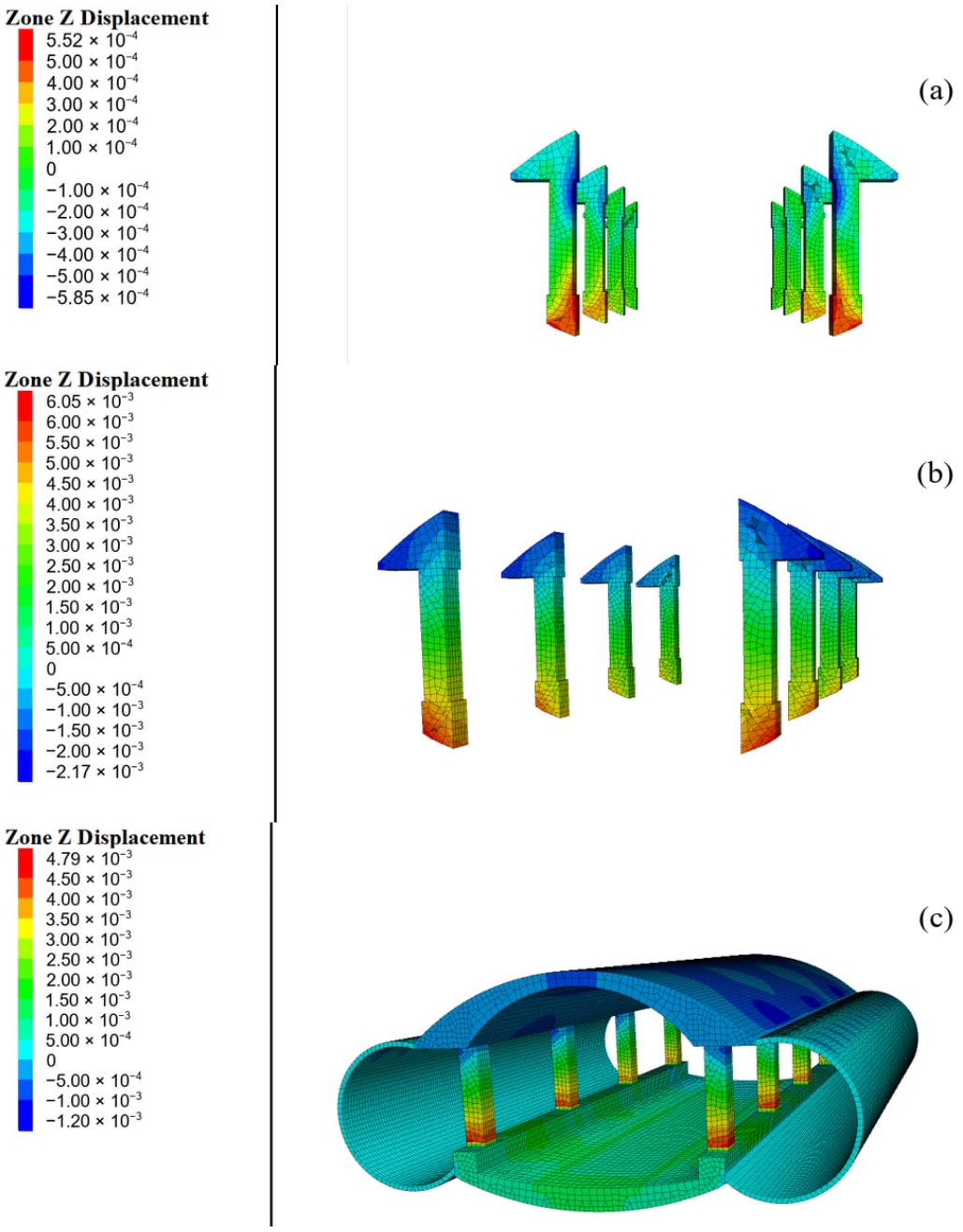


Figure 26. Z-direction displacement contours of the beams and columns at (**a**) S4, (**b**) S6, and (**c**) S8, as defined in Figure 6. Displacement is shown in m, with positive values denoting heave and negative values denoting settlement.

(2) Upon entering the large-section expansion excavation stage of the station, the radial soil constraint is removed, triggering stress redistribution. The beam-column system responds to the changed restraint and support conditions. The stress release from the surrounding rock causes the deformation to rise sharply. The peak displacement at the top longitudinal beam corbels increases to −2.12 mm, while that of the bottom longitudinal beams reaches 4.96 mm. This step produces a substantial displacement increase; the largest reported displacement magnitudes occur after the subsequent segment removal at S6.

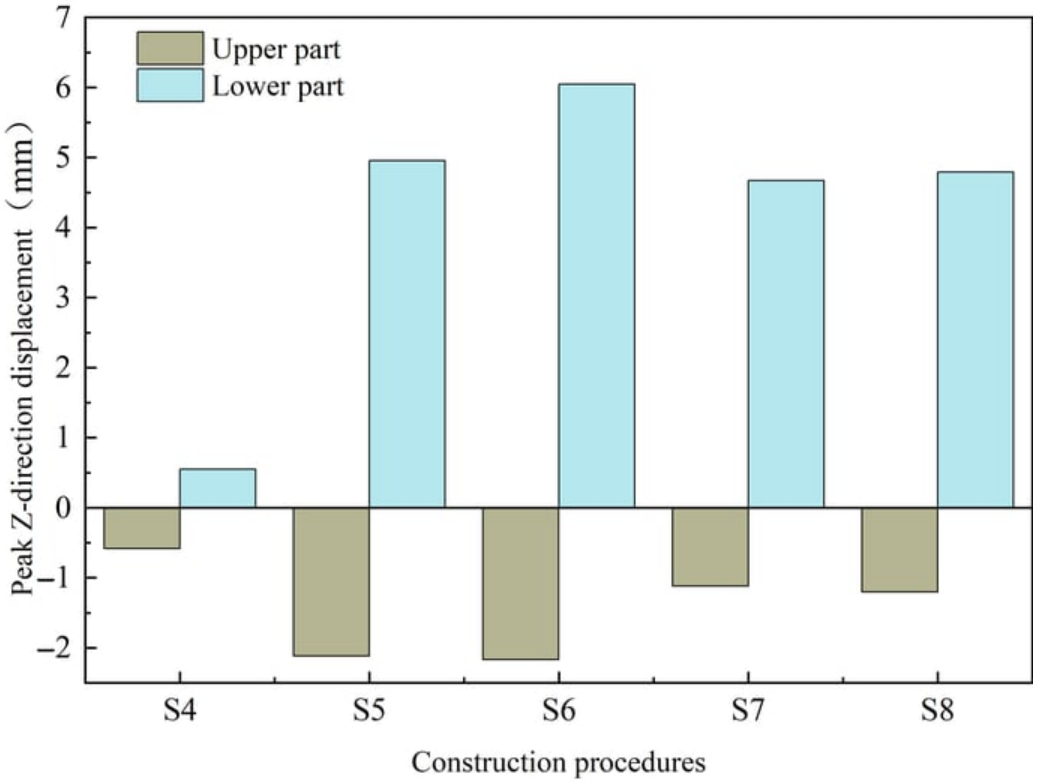


Figure 27. Peak Z-direction displacement of the beams and columns.

Subsequently, removing the remaining segments further weakens the segment support effect. Loads transfer downward through the columns to the bottom longitudinal beams. At this point, the upper-beam settlement increases slightly in magnitude to −2.17 mm. This identifies S6 as the reported control step for upper-beam settlement. However, the peak displacement at the bottom of the bottom longitudinal beams further increases to 6.05 mm.

(3) During the final construction stage, the secondary linings of both the station and the running tunnel successively close to form complete rings. These linings change the stiffness and available load paths of the assembled system. The resulting response reflects interaction among the activated pipe-curtain, segment, beam-column, and lining regions.

At S8, the assembled-system display gives upper- and lower-region displacement extrema of −1.20 mm and +4.79 mm, respectively. These later values reflect redistribution within the changed structural configuration and are considered alongside the preceding S6 connection-displacement peaks. Upper-corbel deformation and lower-beam movement during S5–S6 therefore remain important references for construction control and monitoring.

5. Discussion

Based on the aforementioned mechanical evolution patterns throughout the entire construction process, the stress and deformation concentration zones at each stage can be determined, thereby identifying the structural weak points. These concentration regions provide a basis for targeted connection detailing and construction-stage control.

5.1. Identification of Vulnerable Structural Locations

Table 3 summarizes selected stress and vertical-displacement responses at the identified concentration regions. Each value refers to the listed location and construction step and is not necessarily the extremum of the entire component over the full sequence.

Table 3. Selected responses at structural concentration regions.

Component	Location	Response Quantity	Construction Step	Reported Value
Pipe Curtain	Joints between lower pipe curtain and tunnel segments	Maximum principal stress	Constructing longitudinal beams and station secondary lining	6.16 MPa
	Joints between upper pipe curtain and tunnel segments		Constructing longitudinal beams and station secondary lining	5.48 MPa
	Joints between lower pipe curtain and tunnel segments	Minimum principal stress	Constructing longitudinal beams and station secondary lining	−8.96 MPa
	Joints between upper pipe curtain and tunnel segments		Erecting temporary supports	−7.46 MPa
	Outer side of upper pipe curtain between adjacent columns	Z-direction displacement	Constructing longitudinal beams and station secondary lining	−7.04 mm
	Joints between lower pipe curtain and bottom longitudinal beams	Z-direction displacement	Constructing longitudinal beams and station secondary lining	11.20 mm
Tunnel Segments	Inner side of haunches on the adjacent sides of the two tunnels	Minimum principal stress	Large-section expansion excavation of the station	−7.31 MPa
	Joints between tunnel segments and lower pipe curtain	Maximum principal stress	Large-section expansion excavation of the station	6.02 MPa
	Contact surfaces between invert and temporary supports	Minimum principal stress	Constructing longitudinal beams and station secondary lining	−6.71 MPa
	Invert	Z-direction displacement	Removing temporary supports and constructing secondary lining inside shield tunnel	14.72 mm
Beam-Column System	Corbels of top longitudinal beams at the columns	Maximum principal stress	Removing the remaining removable tunnel segments	3.33 MPa
	Joints between columns and bottom longitudinal beams	Minimum principal stress	Removing the remaining removable tunnel segments	−6.35 MPa
	Bottom of bottom longitudinal beams	Z-direction displacement	Removing the remaining removable tunnel segments	6.05 mm
	Trapezoidal corbels of top longitudinal beams	Z-direction displacement	Removing the remaining removable tunnel segments	−2.17 mm

The controlling construction step varies with the structural component and response quantity. The pipe-curtain maximum principal stress peaks occur at S7, whereas the reported segment tensile-demand peak and upper longitudinal-beam corbel tensile-demand

peak occur at S5 and S6, respectively. The upper-curtain downward displacement and segment invert heave reach their largest reported magnitudes at S8. These differences support separate construction-stage checks for the identified connection regions and deformation-sensitive locations.

5.2. Reinforcement Measures for Critical Locations

The following measures, including the stated dimensions and reinforcement arrangements, are proposed as preliminary detailing options for the critical locations identified by the numerical analysis. Their quantitative effectiveness has not been evaluated through a comparison of the original and strengthened configurations.

5.2.1. Reinforcement Measures for the Pipe Curtain Structure

To address the joint stress concentrations revealed by numerical simulations, joint stiffness should be coordinated with deformation compatibility and load-transfer requirements. A connection detail combining flexible transitions and shear keys is proposed for further design assessment.

Annular shear ribs are proposed to be welded to the outer walls of the steel pipe ends to enhance mechanical interlocking between the steel pipes and the ring-beam concrete and provide resistance to interfacial shear slip. Additionally, a 10 mm groove for an elastic gasket is proposed at the interface between the steel pipes and the tunnel segments. The gasket is intended to accommodate local relative displacement associated with segment rotation. Its deformation capacity should be coordinated with the structural bearing and shear-transfer details of the connection.

After completing the jacking of the lower pipe curtain, a cement–sodium silicate binary slurry is proposed for injection into the over-excavated gaps between the pipe curtain and the soil through reserved grouting holes. The grouting is intended to fill the voids, restore contact with the surrounding ground, and provide additional restraint against subsequent upward movement of the lower pipe curtain. Injection pressure, volume, and sequence should be controlled according to ground conditions and monitored deformation.

5.2.2. Reinforcement Measures for Corbels at Beam-Column Joints

(1) Corbel Reinforcement

In the tension zones of the top longitudinal-beam corbels, two rows of Φ25 diagonal bent-up rebars are proposed as additional tension reinforcement, targeting the elevated tensile demand identified during removal of the remaining segments at S6. The reinforcement orientation and anchorage should follow the connection load path, with the required reinforcement area established through connection-level design checks.

(2) Joint Reinforcement Between Bottom Longitudinal Beams and Pipe Curtain

To address the stress concentration at the joints between the bottom longitudinal beams and the lower pipe curtain, curved steel bearing plates are proposed at their contact surfaces. This arrangement is intended to distribute support reactions over a larger effective area and reduce the concentration of local bearing demand.

A 20 mm-thick neoprene pad is also proposed at the bearing interface before casting the bottom longitudinal beams, to accommodate local rotation and improve contact conformity. The arrangement of the steel plate and pad should be defined as a bearing assembly and checked for compression, shear transfer, and rotational accommodation.

Additionally, the stirrups of the bottom longitudinal beams are proposed to be closely spaced at Φ12@80 mm on both sides of the pipe curtain. The proposed extent of this

closely spaced reinforcement is 1.5 times the local beam height, with its final arrangement determined from the local shear demand and beam geometry.

5.2.3. Construction Process Control of Key Procedures

Regarding the timing of backfill grouting behind the tunnel segments, convergence at the haunches of the adjacent tunnels should be monitored during the large-section expansion excavation of the station. The measured convergence and its rate of change should be assessed against project-specific control criteria. When the specified intervention criterion is reached, compensation grouting into the intermediate soil pillar may be considered following assessment of the ground conditions and structural response. This measure is intended to restore ground confinement and control further deformation around the tunnel segments.

The longitudinal temporary supports should be removed in controlled stages to avoid abrupt loss of support. The proposed construction sequence follows the principle of "staggered removal (removing alternating supports) and provision of replacement support before removal". Before removing a single temporary support, the adjacent station secondary lining at that cross-section should be complete and satisfy the applicable concrete-strength acceptance condition specified in the construction design, consistent with Section 2.3. Structural response should be checked after each removal stage before proceeding to the next stage.

5.3. Comparison with Published Studies

Zhang et al. [32] investigated densely arranged transverse pipe curtains and reported midspan deflections of −4.11 mm and −4.43 mm from an elastic-plate solution and a corresponding finite-element benchmark, respectively. In the present model, the final maximum vertical displacement of the upper pipe curtain is −7.08 mm. These published results provide reference values for discussing the magnitude of pipe-curtain deformation. Zhang et al. also highlighted the contribution of inter-pipe connections to the deformation response during excavation, emphasizing the importance of structural continuity in pipe-curtain support systems.

Bai et al. [33] reported a final ground settlement of 24.1 mm for Shifu Road Station constructed using the small pipe roof-beam method, while the predicted maximum surface settlement in the present study is 6.18 mm. Their study identified transverse pilot-tunnel excavation and excavation of the intervening soil as important settlement-generating stages. The present analysis likewise identifies station excavation and segment removal as key stages of settlement accumulation. These findings provide an engineering reference for interpreting the staged development of ground settlement and highlight the importance of coordinating excavation, segment removal, and support installation.

Because the published cases differ in geometry, ground conditions, construction method, and response definitions, these comparisons provide engineering context rather than independent validation.

5.4. Applicability and Further Work

The model is intended to identify sensitive construction stages and potentially vulnerable structural regions under the adopted modelling conditions. It has not been calibrated or validated against independent field measurements or a reproducible same-condition benchmark. The Mohr–Coulomb model provides a practical engineering representation of staged excavation but does not reproduce stress-dependent stiffness, small-strain nonlinearity, or post-yield hardening and softening. These simplifications may influence the calculated deformation, soil yielding, and load redistribution.

No systematic parameter, mesh-size, or boundary-distance sensitivity analysis was performed. Variations in soil stiffness and strength may affect the calculated displacement, yielding, and structural demand, while mesh refinement and boundary distance may influence local stress peaks and global deformation. The model also represents a post-dewatering condition without groundwater flow, pore-pressure coupling, dewatering-induced ground movement, or surface surcharge. The effects of alternative groundwater and loading conditions were not quantified.

The reinforcement measures proposed in Section 5.2 are preliminary design concepts and were not incorporated into the numerical model. Their effectiveness in reducing local tensile demand or cracking risk has therefore not been demonstrated. Further work should prioritize independent validation, sensitivity analyses, hydro-mechanical modelling, nonlinear connection assessment, and direct comparison of the original and strengthened configurations.

6. Conclusions

Using Baidang South Station as the engineering background, this study examines the circumferential pipe curtain (CPC) method through three-dimensional FLAC3D analysis. The analysis follows ground and structural responses throughout the proposed "three-stage, eight-step" construction sequence. The main conclusions are as follows:

(1) The CPC arrangement connects the existing shield tunnels through upper and lower pipe curtains, forming a pre-support system for subsequent station excavation. The proposed construction sequence coordinates excavation, segment removal, structural installation, and temporary-support removal, providing a framework for examining load redistribution during tunnel-first station construction.

(2) For the modeled condition, the final maximum surface settlement is 6.18 mm at the station centerline, with noticeable settlement concentrated within approximately 50 m of the centerline. Station expansion excavation and removal of the remaining tunnel segments are important stages of settlement accumulation. These operations warrant particular attention when coordinating excavation, support installation, and deformation monitoring.

(3) The pipe-curtain–segment connections remain important stress concentration regions during structural-system transformation. The upper and lower pipe curtains reach peak maximum principal stresses of 5.48 and 6.16 MPa, respectively, during longitudinal-beam and station secondary-lining construction (S7). However, the largest calculated downward displacement of the upper pipe curtain occurs at S8, reaching 7.08 mm. Thus, the controlling construction step should be identified separately for each response quantity.

(4) Station expansion excavation (S5) produces elevated tensile demand near the connections between the tunnel segments and the lower pipe curtain. The calculated local maximum principal stress reaches approximately 6 MPa, exceeding the adopted C50 concrete tensile-strength reference of 1.89 MPa. Its subsequent reduction to 1.82 MPa indicates reduced but persistent local tensile demand. Together with the deformation shift from crown settlement to invert heave, these findings identify the connections and tunnel invert as priorities for construction-stage assessment and monitoring.

(5) Removal of the remaining tunnel segments (S6) is the controlling step for the reported beam-column stress peaks. The upper longitudinal-beam corbels reach a maximum principal stress of 3.33 MPa, exceeding the adopted C40 concrete tensile-strength reference of 1.71 MPa. The column–bottom longitudinal-beam connections reach a minimum principal stress of −6.35 MPa. The concrete tensile-stress comparisons identify locations requiring detailed reinforcement, anchorage, and connection checks. Later reductions in several stress quantities reflect redistribution within the simulated sequence, while the preceding construction-stage demands remain relevant to design assessment.

(6) The identified locations and controlling steps provide a basis for targeted connection detailing and construction control. Proposed options include deformation-compatible connections with shear-transfer details, additional corbel reinforcement, bearing plates and pads, and controlled backfill grouting. These measures are preliminary design considerations whose quantitative effectiveness requires comparison of the original and strengthened configurations. Temporary supports should be removed in controlled stages after completion of the adjacent station lining and satisfaction of the specified concrete-strength acceptance condition. Replacement support should be provided before removal, with structural response checked before proceeding to the next stage.

The findings should be interpreted under the adopted modelling assumptions, while independent validation and quantitative assessment of the proposed strengthening measures remain subjects for further research.

Author Contributions: X.S.: Methodology, Data curation, Visualization, Funding acquisition. M.Z.: Conceptualization, Methodology, Supervision, Writing—review & editing. H.L.: Investigation, Data curation, Software, Writing—original draft. Z.D.: Project administration. H.G.: providing design materials. All authors have read and agreed to the published version of the manuscript.

Funding: This study was funded by the National Key R&D Program of China Grant Nos. 2023YFC3806701.

Data Availability Statement: Data will be made available on request.

Acknowledgments:

Conflicts of Interest: Author Huawei Guo was employed by the company China Railway Siyuan Survey and Design Group. The remaining authors declare that the research was conducted in the absence of any commercial or financial relationships that could be construed as a potential conflict of interest.

References

1. Zare Naghadehi, M.; Thewes, M.; Alimardani Lavasan, A. Face stability analysis of mechanized shield tunneling: An objective systems approach to the problem. *Eng. Geol.* **2019**, *262*, 105307. [CrossRef]
2. Liu, X.X.; Shen, S.L.; Xu, Y.S.; Yin, Z.Y. Analytical approach for time-dependent groundwater inflow into shield tunnel face in confined aquifer. *Int. J. Numer. Anal. Methods Geomech.* **2018**, *42*, 655–673. [CrossRef]
3. Zhu, C. Control of surface settlement by considering shield tunneling technology. *KSCE J. Civ. Eng.* **2017**, *21*, 2896–2907. [CrossRef]
4. Feng, J.; Song, J.; Li, Y.; Zhang, X.; Zhang, J.; Nie, L.; Yan, Z. Mechanical behavior analysis of station construction by the tunnel-before-station pile method. *KSCE J. Civ. Eng.* **2026**, *30*, 100445. [CrossRef]
5. Liang, J.; Su, W.; Liu, T.; Wu, H.; Lu, L.; Zhong, H.; Zhou, S. Analysis of large deformation characteristics of deep foundation pit at a subway station constructed by the tunnel-before-station method. *Eur. J. Environ. Civ. Eng.* **2025**, *29*, 3800–3827. [CrossRef]
6. Brasov, C.H.; Qian, Q.H.; Qi, C.Z., Translators; *Essence of Subway Construction in Russian*; China Railway Publishing House: Beijing, China, 2002.
7. Xiong, Q. Construction technology for subway stations using the tunnel-first method. *Railw. Stand. Des.* **2009**, *53*, 106–111. (In Chinese) [CrossRef]
8. Liu, J.; Qi, T.; Wu, Z. Analysis of ground movement due to metro station driven with enlarging shield tunnels under building and its parameter sensitivity analysis. *Tunn. Undergr. Space Technol.* **2012**, *28*, 287–296. [CrossRef]
9. Yan, M.; Yang, X.R.; Li, A.M.; Wang, W.J.; Ding, D.Y. Comparative analysis of schemes for metro station built by enlarging large-diameter shield tunnel. *Adv. Mater. Res.* **2012**, *368–373*, 2731–2735. [CrossRef]
10. Zhou, J.; Shu, P.; Zhang, B.; Deng, B.; Wu, Y. A finite element analysis of tunnel lining demolition by blasting for subway tunnel expansion. *Appl. Sci.* **2022**, *12*, 9564. [CrossRef]
11. Liu, W.N.; Lu, M.L.; Zhang, X.J.; Li, Z.P. Model test on metro station constructed by combination of shield method and shallow-buried tunneling method. *Chin. J. Rock Mech. Eng.* **2009**, *28*, 1629–1639. (In Chinese)
12. Liu, J.; Wang, F.; He, S.; Wang, E.; Zhou, H. Enlarging a large-diameter shield tunnel using the Pile–Beam–Arch method to create a metro station. *Tunn. Undergr. Space Technol.* **2015**, *49*, 130–143. [CrossRef]

13. Zhang, M.; Liu, Y.; Fan, L.; Li, P. Performance of constructing a double-deck subway station by combining the shield method and cavern–pile method. *Tunn. Undergr. Space Technol.* **2017**, *67*, 120–131. [CrossRef]
14. Sedghi, M.; Golshani, A. Impact of pile–beam–arch tunnel enlargement method on ground movements and building damage. *Geotech. Geol. Eng.* **2024**, *42*, 2361–2386. [CrossRef]
15. Zhang, D.L. Essential issues and their research progress in tunnel and underground engineering. *Chin. J. Theor. Appl. Mech.* **2017**, *49*, 3–21. (In Chinese) [CrossRef]
16. Chen, Y.; Teng, J.; Sadiq, R.A.B.; Zhang, K. Experimental study of bolt-anchoring mechanism for bedded rock mass. *Int. J. Geomech.* **2020**, *20*, 04020019. [CrossRef]
17. Wu, B.; Wang, X.; Bai, J.; Liu, S.; Wang, G.; Li, G. A study of the anchorage body fracture evolution and the energy dissipation rule: Comparison between tensioned rock bolts and torqued rock bolts. *Adv. Civ. Eng.* **2021**, *2021*, 5542569. [CrossRef]
18. Jiang, Y.; Luo, H.; Liu, H.; Gu, J. Mechanical study on leading ductule and pipe roof pre-support technologies in tunnel excavation. *Buildings* **2025**, *15*, 3791. [CrossRef]
19. Zhang, B.; Wang, J.P.; Wang, F.M.; Dong, X.P. Effect of advance small-diameter pipes on tunnel face stability. *J. Zhengzhou Univ. (Eng. Sci.)* **2009**, *30*, 30–34. (In Chinese)
20. Zhu, J.; Zhang, Y.; Tao, L.; Wang, N.; Su, L.; Zhang, J.; Zhao, X.; Xu, Y. A case study of deformation and failure of existing building induced by pipe jacking with pipe roof method. *Tunn. Undergr. Space Technol.* **2026**, *169*, 107301. [CrossRef]
21. Guan, X.; Wang, R.; Fu, H.; Feng, W.; Jin, X.; Li, S.; Xu, S.; Li, J. Settlement analysis of ground surface and adjacent building caused by driving and expansion excavation of shield tunnel using artificial freezing method. *Sustainability* **2023**, *15*, 14166. [CrossRef]
22. Hong, Z.; Fu, S.; Wu, Y.; Zhang, Y.; Lu, L. Numerical research on the impact of horizontal freezing on existing underground structures in shield reception. *Front. Earth Sci.* **2025**, *12*, 1511744. [CrossRef]
23. Yang, S.S.; Zhang, D.W.; Wang, M.; Xu, J.M.; Shen, C.; Zhang, C.Z. Ground settlement caused by pipe-roof pre-construction method: Effect of the sequence of jacking pipe groups. *J. Cent. South Univ.* **2024**, *31*, 576–588. [CrossRef]
24. Xie, X.; Zhao, M.; Shahrour, I. Experimental study of the behavior of rectangular excavations supported by a pipe roof. *Appl. Sci.* **2019**, *9*, 2082. [CrossRef]
25. Zhang, X.; Qin, J.; Zhang, X.; Zhang, J.; Jiang, X. Monitoring and simulation of ground deformations by super-large EPB culvert jacking tunnelling combining with pipe-roof preconstruction method (PPM) in urban environments. *Tunn. Undergr. Space Technol.* **2025**, *165*, 106909. [CrossRef]
26. Fu, J.; Ning, M.; Zhang, J.; Fan, Z.; Fu, J.; Wu, Y.; Jin, X.; Feng, J.; Liu, Y. Construction disturbance effects of tunnelling in completely decomposed granite and reinforcement using interlocked pipe roofs. *Geotech. Geol. Eng.* **2026**, *44*, 143. [CrossRef]
27. Zhang, X.; Wu, S.; Li, L.; Wang, J.; Tong, S.; Li, X.; He, Z. Calculation method for earth pressure and deformation of transverse pipe roof considering micro-arching effect. *KSCE J. Civ. Eng.* **2026**, *30*, 100306. [CrossRef]
28. Wang, X.Y.; Liu, W.N.; Zhao, B.M.; He, M.D.; Li, K.M. Pre-cutting technology and key technical issues in its application. *Mod. Tunn. Technol.* **2011**, *48*, 22–27. (In Chinese)
29. Li, P.; Liu, X.; Jiang, X.; Zhang, X.; Wu, J.; Chen, P. Investigation of the first quasi-rectangular metro tunnel constructed by the 0-θ method. *Front. Struct. Civ. Eng.* **2023**, *17*, 1707–1722. [CrossRef]
30. Bai, Q.; Zhao, W.; Ni, P.; Li, J.; Jia, P.; Liu, X.; Li, T. Theoretical model for predicting deformation of pipe curtain support structure in underground engineering. *Eng. Struct. Civ. Eng.* **2026**, *20*, 246–261. [CrossRef]
31. *GB 50010-2010*; Code for Design of Concrete Structures. China Architecture & Building Press: Beijing, China, 2011. (In Chinese)
32. Zhang, Y.; Tao, L.; Dong, L.; Zhao, X.; Bian, J.; An, S.; Chen, X. Theoretical analysis of horizontal pipe curtains with tight rows. *Chin. J. Geotech. Eng.* **2021**, *43*, 365–374. [CrossRef]
33. Bai, Q.; Zhao, W.; Zhang, Y.; Jia, P.; Meng, X.; Lu, B.; Wang, X.; Sun, D. Construction of shallow buried large-span metro stations using the small pipe roof-beam method. *Front. Struct. Civ. Eng.* **2024**, *18*, 122–136. [CrossRef]

Disclaimer/Publisher's Note: The statements, opinions and data contained in all publications are solely those of the individual author(s) and contributor(s) and not of MDPI and/or the editor(s). MDPI and/or the editor(s) disclaim responsibility for any injury to people or property resulting from any ideas, methods, instructions or products referred to in the content.